

**Significance of gasification during oxy-fuel combustion of a lignite char in a fluidised
bed using a fast UEGO sensor**

Marco A. Saucedo^{a,*}, Mathias Butel^a, Stuart A. Scott^a, Nick Collings^a, John S. Dennis^b

^a *University of Cambridge, Department of Engineering, Trumpington Street, Cambridge, CB2 1PZ,
United Kingdom*

^b *University of Cambridge, Department of Chemical Engineering and Biotechnology, New Museums
Site, Pembroke Street, Cambridge, CB2 3RA, United Kingdom*

***Corresponding author**

Marco A. Saucedo

Department of Engineering

University of Cambridge

Trumpington Street

CB2 1PZ, Cambridge

United Kingdom

Phone: +44 12233 32645

E-mail: mas225@cam.ac.uk

Abstract

In oxy-fuel combustion, fuel is combusted in a mixture of O₂ and recycled flue gas, *i.e.* the N₂ is replaced by CO₂ with the O₂ supplied from an air separation unit. The resulting gas consists largely of steam and CO₂, which would be ready for sequestration when dried. In this work, the rate of reaction of particles of lignite char, typically 1200 μm diameter, in a fluidised bed reactor was determined using mixtures of O₂ with either CO₂ (“oxy-fuel”) or N₂. A universal exhaust-gas oxygen (UEGO) sensor enabled rapid measurements of the oxygen partial pressures in the off-gas, representing a novel application of this type of sensor. It was found that the rate of combustion of the particles in oxy-fuel is much more sensitive to temperature than in the equivalent O₂ and N₂ mixture. This is because for bed temperatures > ~1000 K particle combustion in mixtures of N₂ and O₂ is rate controlled by external mass transfer, which does not increase significantly with temperature. In contrast, using oxy-fuel, as the temperature increases, gasification by the high concentrations of CO₂ present becomes increasingly significant. At low temperatures, *e.g.* ~1000 K, rates of combustion in oxy-fuel were lower than those in mixtures of O₂ and N₂ containing the same mole fraction of O₂ owing, primarily, to the lower diffusivities of O₂ in CO₂ compared to O₂ in N₂ under conditions at which external mass transfer is still a significant factor in controlling the rate of reaction. At higher temperatures, *e.g.* 1223 K, oxy-fuel combustion rates were significantly higher than those in O₂ and N₂. The point at which oxy-fuel combustion becomes more rapid than in mixtures of O₂ and N₂ depends not only on temperature but also on the ratio of O₂ to CO₂ or N₂, respectively. A numerical model was developed to account for external mass transfer, changes in the temperature of the particle and for the effect of gasification under oxy-fuel conditions. The model confirmed that, at high temperatures, the high concentration of CO₂ at the surface of the burning particle in the oxy-fuel mixture led to an increase in the overall rate of carbon conversion *via* $\text{CO}_2 + \text{C} \rightarrow 2\text{CO}$, whilst the rate of reaction with O₂ was limited by mass transfer. Good agreement was observed between the rates predicted by the numerical model and those observed experimentally.

Keywords

Combustion; Oxy-fuel; Gasification; Coal; CO₂ capture; UEGO sensor.

Nomenclature

c or C^*	concentration of active sites per unit mass of carbon, g^{-1}
C_T	total concentration in the fluidised bed, mol m^{-3}
$D_{i,j}$	binary diffusivity, involving species a in b , $\text{m}^2 \text{s}^{-1}$
$D_{i,j}^{eff}$	effective diffusivity in a fluidised bed, $\text{m}^2 \text{s}^{-1}$
D	mean diffusivity, $\text{m}^2 \text{s}^{-1}$
d_a	diameter of a sand particle, m
$d_{b,m}$	mean diameter of a bubble, m
d_p	diameter of a char particle, m
E_{k_{-1}/k_1}	activation energy for the rate constant k_{-1}/k_1 , kJ mol^{-1}
g	gravitational acceleration, m s^{-2}
h	heat transfer coefficient from the particle to the bed, $\text{W m}^{-2} \text{K}^{-1}$
ΔH_i	enthalpy of reaction i , kJ mol^{-1}
H	expanded height of the fluidised bed, m
H_{mf}	height of the fluidised bed at minimum fluidisation, m
J_i	molar flux of species i , $\text{mol m}^{-2} \text{s}^{-1}$
k_1, k_{-1}	rate constants of gasification per active site, $\text{mol s}^{-1} \text{bar}^{-1}$
k_2	rate constant of gasification per active site, mol s^{-1}
k_g	mass transfer coefficient for a reactant towards a reacting particle, as well as for products away from it, m s^{-1}
K_p	equilibrium constant for the overall gasification reaction $\text{C} + \text{CO}_2 = 2\text{CO}$, -
m_{batch}	mass of a batch of char, g
M_i	molar mass of species i , g mol^{-1}
\dot{N}	total molar flow rate through the bed, mol s^{-1}
p_i	partial pressure of gaseous species i , bar
P	total pressure, bar
Q	rate of consumption of carbon per particle, mol s^{-1}
R_p	Initial radius of a char particle, m
R	universal gas constant, $\text{kJ mol}^{-1} \text{K}^{-1}$
R'_g	rate of gasification of char per unit mas of sample, $\text{mol s}^{-1} \text{g}^{-1}$
R''_g	gasification rate expressed as f lux, $\text{mol m}^{-2} \text{s}^{-1}$
$R'_{c,0}$	overall carbon rate at zero conversion, $\text{mol s}^{-1} \text{g}^{-1}$
R''_c	rate of carbon conversion of a single particle of char, $= R'_{c,0} (V_p \rho_e)$, mol s^{-1}
Re_p	Reynolds number in the particulate phase $= U_p d_p / \nu$, -
Sc	Schmidt number $= \nu / D$, -

Sh	Sherwood number = $d_p k_g / D$, -
Sh_{EMCD}	Sh for equimolar counter-diffusion of reactant and product, -
t	time, s
T	temperature, K
T_b	temperature of the fluidised bed, K
T_p	temperature of the particle, K
ΔT	temperature change between the particle and the bed = $T_p - T_b$, K
U	superficial fluidising velocity, m s^{-1}
U_b	rise velocity of a bubble, m s^{-1}
U_{mf}	minimum superficial fluidising velocity, m s^{-1}
X	conversion of carbon, -
V_p	volume of a single particle of char, m^3
y_i	mole fraction of species i , -
$y_{i,bulk}$	mole fraction of species i in the bulk phase, -
$y_{i,s}$	mole fraction of species i at the surface of the particle, -

Greek letters

γ	ratio of the molar fluxes of CO to CO ₂ at the surface of the particle = $J_{\text{CO},s} / J_{\text{CO}_2,s}$, -
δ	thickness of the mass transfer boundary layer, m
ε	void in the fluidised bed, -
ε_b	void fraction owing to bubbles in the fluidised bed, -
ε_{mf}	void fraction in a bed at minimum fluidisation, -
ε_r	emissivity of the particle, -
η	effectiveness factor of the extent of mass transfer limitations within the particle, -
ξ_i	mass rate of production of species i based on volume unit of bed, $\text{mol m}^{-3} \text{s}^{-1}$
ρ_e	density of a particle of char before reaction, g m^{-3}
σ	Stefan-Boltzmann constant, $\text{W m}^{-2} \text{K}^{-4}$
σ_r	dimensionless radius = r/R_p , -
τ^2	tortuosity factor of the region around the particle of pellet, -
ϕ	stoichiometric coefficient of the global chemical equation for oxidation of carbon
φ	mass fraction of carbon in the char, -
Φ_L	modified Thiele modulus [56], -
χ_1	fraction of the carbon which oxidises to CO ₂ sufficiently close to the particle of char to transfer all its heat of reaction to the particle = $1/(1 + \gamma)$, -
χ_2	fraction of the carbon which oxidises to CO <i>via</i> the gasification reaction = $(0.5 \times R'_{g,0}) / R'_{c,0}$, -

Abbreviations

BET	Brunauer-Emmett-Teller
CCS	carbon capture and storage
FBC	fluidised bed combustion
GHG	greenhouse gas
pf	pulverised fuel
UEGO	universal exhaust gas oxygen

1. Introduction

The combustion of fossil fuels such as coal to generate electricity contributes substantially to the total anthropogenic emission of carbon dioxide [1]-[3]. To meet the projected demand for electricity it is unlikely that this use of fossil fuels can be replaced by renewable sources of energy, such as wind, solar or biomass, over the next two decades [4]. Accordingly, because of the link between the concentration of CO₂ in the atmosphere and climate change, means are needed to be able to continue using coal whilst capturing the CO₂ generated and sequestering it in suitable geological structures [5], commonly referred to as Carbon Capture and Storage (CCS). Though no proven CCS technique has yet been proven at scale, the economics of CCS are much enhanced if only CO₂ is the gas to be captured.

There are two main methods of burning coal for power generation: pulverised coal combustion (pf) and fluidised bed combustion (FBC). Currently, about 97% of the world's coal-fired plants use pulverised coal [6], but there has recently been renewed interest in fluidised beds. This is because fluidised bed combustion is less sensitive to coal quality, and has attractive characteristics with respect to noxious emissions amelioration. There will perhaps also be a trend towards co-firing with biomass, but transport costs may limit its use to power stations of around 400-500 MW (thermal), a size not necessarily suitable for new pf plant, but viable for FBCs. Fluidised beds also lend themselves to pressurised operation (unlike pf plant), and then the char within the bed reduces nitrogen oxides to molecular N₂ so that the inherent levels of NO_x from FBCs are potentially less than from pf boilers [7].

One technique for creating an off-gas stream of virtually pure CO₂ is to use oxy-fuel combustion. Here, the fuel is burned in a mixture of oxygen and CO₂, rather than air, resulting in an off-gas containing mainly CO₂ and H₂O. Combustion with pure O₂ would result in too high a flame temperature, necessitating recycling of some CO₂. Air separation plant is required to produce the O₂, and the flue gases must be compressed for recycling, thus reducing the efficiency of a pulverised fuel (pf) fired plant with a conventional steam cycle from ~40% to ~29% [8]. However, the advantages of this technology are (i) both combustion and air separation technology are well developed, (ii) conventional furnaces using air can probably be retrofitted to use mixtures of oxygen and CO₂, and (iii) reduced NO_x emissions. The latter advantage arises from (a) less thermal NO_x because gaseous N₂ is absent, and (b) the chemical reduction of fuel-derived NO_x when a proportion of the CO₂-rich flue gases is recycled in order to dilute the incoming pure oxygen [8]. Whilst oxy-fuel has been demonstrated in pulverised fuel burners [9]-[18], less work has been done using this technique in FBCs (*e.g.* [19]-[31]) and little has been published on the fundamental mechanisms of combustion using oxy-fuel in a fluidised bed (*e.g.* [32]-[33]). Accordingly, this paper is concerned with an experimental and theoretical investigation of the rates of combustion of a lignite char in a bubbling

fluidised bed, fluidised using either air or oxy-fuel. Particular attention has been paid to factors affecting the reaction rate in oxy-fuel as compared to air.

2. Experimental

2.1. Materials

Fuel and preparation of the char. A char prepared from a low-rank Hambach lignite coal, supplied by RWE Power AG, Germany, was investigated in this work, and has been described previously ([6],[34],[35]). The lignite char was prepared from its parent lignite by pyrolysis in nitrogen in a fluidised bed of sand at 1073 K. The reactor had an inside diameter of 78 mm and was made from 316 stainless steel. A detailed description of the apparatus and the experimental method have been given elsewhere ([6], [34]). The elemental analysis (CHN analysis) of the char, together with its ash content, is shown in Table 1. The initial BET area was about $235 \text{ m}^2 \text{ g}^{-1}$. Finally, the char was sieved to six different size fractions: 600-710, 710-850, 1000-1400, 1400-1700, 1700-2360 and 2360-2800 μm .

[Table 1 hereabouts]

2.2. Apparatus and Method

Batch experiments were performed in a fluidised bed made of quartz of i.d. 125 mm and length 610 mm, provided with a porous frit as the distributor (with pressure drop sufficient to ensure uniform fluidisation), situated 220 mm from the base of the reactor. A narrower section at the top of the reactor, i.d. 40 mm and length 190 mm, increased the gas velocity leaving the bed to prevent ingress of air. A schematic diagram of the general arrangement of the apparatus is shown in Figure 1. The reactor was externally heated by an electric furnace. The temperature of the bed was measured by a K-type thermocouple (1.5 mm dia.) inserted into the top of the bed (with the tip situated 50 mm above the distributor plate), and the furnace controlled the bed temperature at the desired value. Air or oxy-fuel was supplied through a connection at the base of the reactor. Dry, high-purity gases, supplied in cylinders by BOC plc., were used with a moisture content $< 20 \text{ ppm}$, because the rate of combustion of CO in air depends on $[\text{H}_2\text{O}]^{0.5}$ [36]. The flow rates of oxygen, nitrogen and carbon dioxide were controlled with rotameters calibrated at 293 K and 1 barg. A steady fraction of the off-gases leaving the reactor, $\sim 50 \text{ cm}^3 \text{ s}^{-1}$ (293 K, 1 bar), was sampled through a capillary of internal diameter 1.0 mm, the exit of which was introduced to a universal exhaust gas oxygen sensor (UEGO Bosch LSU 4.9), described in Section 2.2.1. The UEGO sensor was housed in a custom-made remote sampling head connected to an in-house electronic system [37]. The tip of the sampling capillary was placed about 150 mm above the top of the bed to minimise the chance of sand being drawn into the sampling line.

[Figure 1 hereabouts]

In a typical experiment, the reactor was filled with 1000 cm³ of pure silica sand (David Ball Group plc, moisture content < 0.1%, sieved to +355,-425 μm). The reactor was then heated to the desired temperature, *viz.* 1023 – 1223 K. The mole fraction of O₂ in the fluidising gas was typically 20.9 mol.% with the balance N₂ or CO₂. The total volumetric flow rate was ~715 cm³ s⁻¹ (at 293 K, 1 bar), giving $U/U_{mf} \sim 3.4 - 4.5$ at $T = 1023 - 1223$ K, with U being the superficial velocity at the temperature of the bed and U_{mf} the superficial velocity at incipient fluidisation, calculated from the correlation of Wen and Yu [38]. Then, a known mass of fuel, typically 0.25 g, was added to the reactor and allowed to react completely. For each set of experimental conditions, at least three tests were performed. The amount of fuel added to the bed was adjusted to avoid complications arising from mass transfer between the bubble and the particulate phases (as described in section 4.1). The time for the batch burn-out of fuel was typically between 60 and 600 s. In some particular experiments, the inlet mole fraction of O₂ was reduced to 2.5 mol.%, balance N₂ or CO₂, with a total volumetric flow rate of ~600 cm³ s⁻¹ (at 293 K, 1 bar), giving $U/U_{mf} \sim 2.8 - 3.8$ at $T = 1023 - 1223$ K.

2.2.1 The UEGO Sensor

Determining the rate of carbon conversion in an oxy-fuel system usually requires measurement of the concentration of two of the species in the outlet to allow a full carbon balance, (*e.g.* [CO₂] and [CO], or [O₂] and [CO], *e.g.* [39]). In addition, whilst measurements of gasification rates are possible with relatively slow sensors (*e.g.* typical, commercially-available infra-red analysers [35]), measurement of combustion rates in O₂, especially for small particles of char ($d_p < 1000$ μm) requires a sensor with a time constant of the order of 0.1 s (*e.g.* [40]). In this work, a UEGO sensor was used, because it is a well-established device for the measurement of relative ratios of air and fuel in internal combustion engines. With a response time of 12 – 20 ms [41], the UEGO is fast enough for the experiments with the fluidised bed. Details of other applications may be found in numerous texts (*e.g.* [42],[43]). A detailed description of the mode of operation can be found elsewhere [37],[41],[44].

The UEGO sensor responds not only to the oxygen concentration, but also to any reactable gases such as CO in the off-gas leaving the fluidised bed. Whilst at first this may seem problematic, the fact that the sensor responds to CO, means that only one measurement is required for a full carbon balance. The UEGO response to CO in the off-gas is as follows: once inside the cavity of the sensor, CO is rapidly oxidised to CO₂ on the platinum electrode according to a catalysed form of the reaction: $\text{CO}_{(g)} + \frac{1}{2}\text{O}_{2(g)} \rightarrow \text{CO}_{2(g)}$. This reaction removes half a mole of O₂ for every mole of CO, so, everything else being equal, the amount of oxygen pumped into the measurement cavity to maintain the partial pressure of O₂ at the control point is increased. Since the sensor returns a voltage proportional to the oxygen pump current, the UEGO accordingly should operate as a total combustion meter, returning a voltage reflecting the oxygen concentration which would obtain if all the carbon had been oxidised immediately to CO₂ in the bed. (In fact in the “normal” automotive use of the

UEGO sensor this is a pivotal characteristic.) To test this hypothesis, the following three cases were tested experimentally:

- *Case 1:* starting with 80 mol.% N₂ and 20 mol.% O₂ (and no CO) the concentrations of CO and O₂ were increased in line with the stoichiometric ratio given by Reaction (4) , below (e.g. 0.6 mol% CO, 20.3 mol% O₂, 79.1 mol% N₂). The balance remained N₂. Thus the effect of the full oxidation of the CO on the platinum catalysts should be to return the mixture as being almost 20 mol.% O₂ in a mixture of N₂ and CO₂. The percentages of CO, and hence CO₂, present are so small compared with the N₂ that the fact that Reaction (4) is not equimolar should not matter.
- *Case 2:* starting again with 80 mol.% N₂ and 20 mol.% O₂, the concentration of CO was increased but this time the concentration of O₂ was held constant with the balance being N₂ (e.g. 0.6 mol% CO, 20 mol% O₂, 79.4 mol% N₂).
- *Case 3:* same as *Case 2* but started with 79.5 mol% N₂ and 20.5 mol% O₂ and involved adding CO while holding the concentration of O₂ constant (e.g. 0.6 mol% CO, 20.5 mol% O₂, 78.9 mol% N₂).

The voltage output from the UEGO sensor for these three cases was plotted in Figure 2. For comparison, the voltage output was also predicted using the diffusion model proposed by [37]. It is apparent that the variation in V_{out} with the concentration of CO in *Case 1* is negligible compared with the change in output obtained by increasing concentration of O₂ by just half a percentage point (*Case 2* to *Case 3*). This supports the view that the UEGO sensor's response to CO is dominated by the near instantaneous Reaction (4) on the surface of the electrodes. In fact, the behaviour of a UEGO sensor when exposed to a mixture of CO and CO₂ is of great practical use.

[Figure 2 hereabouts]

One useful consequence of this is that the mole fraction of N₂ in the cavity is always the same as the mole fraction being fed into the reactor when the bed is fluidised in a mixture of O₂ and N₂, because the net effect across the bed and the platinum electrodes is that each mole of O₂ removed by reaction with carbon is replaced by a mole of CO₂.

3. Theory

To a first approximation, char conversion is described by the following global chemical reactions:





Reactions (1), (2) and (3) occur only at surfaces, which may include active sites inside the porous structure of the char. Crucially the analysis that follows treats the combustion reactions, (1) and (2), and the gasification reaction, (3), as being independent.

Three effects are known to control the overall rate of combustion: (i) the transport of species across the gaseous boundary layer surrounding the particle, (ii) the transport of species within the porous structure of the char particle and (iii) the kinetics of the reactions (*i.e.* 1-4). The intrinsic kinetics of the reactions with oxygen are usually sufficiently fast that allowance must be made for mass transfer. Here, these effects are taken into account by solving the equations governing mass transfer external to the particle in order to calculate the surface concentration of CO_2 , and assess the contribution of the gasification reaction, (3), to the overall rate of char conversion. As discussed below, the reaction with O_2 is so fast that it is limited by external mass transfer for the char, temperature and range of particle sizes used. Since this paper is concerned with the combustion of batches of char within a fluidised bed, it is further assumed (i) that the amount of reactant consumed during the reaction is sufficiently small for the bulk gases in the particulate phase to be at the inlet concentration, and (ii) there is no cross flow limitation. To avoid complications arising from the shrinkage and evolution of pore structure in the char during conversion, only the initial rate of combustion is considered.

3.1. Combustion kinetics

It is generally accepted that both CO and CO_2 are primary products, presumably produced at wholly different active sites [45]. However, there remain fundamental difficulties in distinguishing between primary CO_2 and that produced by rapid oxidation of CO in the high temperature region close to the particle. Arthur [46] studied the combustion of two carbons of widely-different reactivities, using a flow method, with POCl_3 vapour added to the oxidising gas to suppress the oxidation of CO. The ratio of the rates at which CO and CO_2 are produced at a carbon surface (*i.e.* the ratio of the rates of reactions (1) and (2)) was found [46] to be given by

$$\frac{J_{\text{CO},s}}{J_{\text{CO}_2,s}} = 2500 \exp\left[-\frac{6240}{T}\right]. \quad (5)$$

where $J_{i,s}$ is the molar flux of species i at the surface of the particle. This ratio was independent of (i) the burning time, *i.e.* the diameter of the carbon particles between 1000 to 2800 μm , (ii) the air velocity (for $T < 1173 \text{ K}$), and (iii) the initial partial pressure of oxygen in the range 0.05 – 0.25 bar. This result excludes the effect of CO_2 reacting with the solid carbon, Reaction (3), because experiments were conducted at temperatures where gasification is negligible compared to combustion

in air. A later work [47] supported Eq. (5), although other studies have suggested that the exact ratio depends on the type of fuel as well as the particle diameter and the oxygen partial pressure at the surface [47]. It is also worth noting that the presence of impurities in the char has been found to favour the production of CO₂ [48]. Nevertheless, Eq. (5) appears to be a good approximation.

For a particle at a typical bed temperature, 1073 K, Eq. (5) implies that the ratio of CO to CO₂ is greater than 7:1. Ordinarily, a large proportion of this CO would be further oxidised to CO₂ in the mass transfer boundary layer. The two most likely intermediate steps in this secondary reaction both involve hydrogen-containing radicals [45]:



It has been shown that a fluidised bed filled with silica sand inhibits Reaction (4) probably by providing a large surface area on which these radicals can recombine [49],[50]. Below ~1023 K, negligible combustion of CO is thought [50] to occur in air anywhere in the bed but CO can still burn above the surface of the fluidised sand. Above ~1073 K, combustion also occurs in the bubbles that form within the bed but there is still little or no combustion in the particulate phase. For a fluidised bed operating at minimum fluidisation there are, theoretically, no bubbles. In practice, however, it is necessary to operate a bed significantly above this minimum mainly because it is the bubbles that are responsible for ensuring that the bed is well mixed. Nevertheless, the bubbles constitute a small fraction of the total bed volume and it is known that a particle spends only a small fraction of its time in contact with a rising bubble [51],[52].

On this basis, and also because the gases used were dry, it has been assumed that the conditions are such that the kinetics of CO oxidation in the gas phase will be slow. Thus, a significant share of the enthalpy change of CO combustion ($\Delta H_{(4)} = -283 \text{ kJ mol}^{-1}$) is released well away from the particle, either in the bubbles or in the freeboard. As a result, the temperature rise associated with the combustion of the particle will not be marked, especially given that the main product of combustion at the surface of the particle is CO ($\Delta H_{(1)} = -111 \text{ kJ mol}^{-1}$ compared with complete combustion of carbon, $\Delta H_{(2)} = -394 \text{ kJ mol}^{-1}$) and the bed has a high specific heat capacity and is well-mixed. To verify this assumption, an energy equation has been considered in this paper to account for changes in the temperature of the particle. This is discussed further in Section 5.1.

3.2. Gasification kinetics

It is generally considered that Reaction (3) is insignificant for FBC in air at typical operating temperatures (1073 – 1273 K). However, under oxy-fuel conditions there is a much higher concentration of CO₂ so that Reaction (3) might be more significant than for combustion in air. It should be noted that here the gasification of the char by water vapour has been neglected because there is little hydrogen in the char and no moisture in the fluidising gases. The most widely-accepted

mechanism for the gasification of carbon by CO₂, Reaction (3), is the oxygen exchange scheme proposed by Ergun [53] leading to

$$R'_{g,0} = \frac{2ck_2(p_{\text{CO}_2,s})}{p_{\text{CO}_2,s} + \left(\frac{k_2}{k_1}\right) + \left(\frac{k_{-1}}{k_1}\right)p_{\text{CO},s}} \quad (8)$$

Here, k_1 , k_{-1} and k_2 are the rate constants per active site, c is the concentration of active sites per unit mass of sample and $p_{i,s}$ is the partial pressure of species i at the surface of the particle. The equilibrium constant k_{-1}/k_1 for three types of carbon is best given by [53]

$$k_{-1}/k_1 = 2.4 \times 10^{-4} \exp\left[-E_{k_{-1}/k_1}/RT\right] \quad (9)$$

with the activation energy $E_{k_{-1}/k_1} = -95 \text{ kJ mol}^{-1}$, although it varies somewhat with the type of carbon [54].

Saucedo *et al.* [35] characterised the char used in this study and found the Ergun expression to give a reasonable fit to the measured rates between 1048 and 1248 K. A summary of the kinetic parameters [35] is given in Table 2.

[Table 2 hereabouts]

3.3. Intra-particle mass transfer

It is important to consider the effect of intra-particle diffusion within a reacting particle of char. In the general case, diffusion of oxygen into the centre of the char can influence the overall rate of reaction. However, for highly reactive carbons, such as those formed from low rank coals (*e.g.* lignite), combustion tends to be diffusion controlled [55], implying reaction at the surface of the particle which therefore shrinks with constant density. Thus it was assumed here that oxygen does not diffuse significantly into the centre of the particle because it reacts immediately on the external surface: this is discussed further in Section 5.2. The same is not true for the slower gasification reaction where CO₂ is present at the surface of the particle in significant concentrations and, therefore, has the opportunity to diffuse into the centre. Brown *et al.* [34] calculated the modified Thiele modulus using the method outlined by [56] for a Langmuir-Hinshelwood rate expression: the calculation was based on experimental measurements of the mass transfer coefficient during gasification of Hambach lignite char particles at 1073 K. The value of $\Phi_L = 0.12$, for $d_p = 1200 \mu\text{m}$, was comfortably below the critical value of 0.3, above which internal diffusion becomes significant. This was confirmed using the Cylindrical Pore Interpolation Method (CPIM) [35], a multicomponent flux model based on the Stefan-Maxwell equations, modified by a momentum balance [57], to describe the diffusion and advective transport within the particle. In [35], intra-particle mass transfer

limitations were not significant at temperatures below 1123 K. However, at higher temperatures, *i.e.* $T > 1173$ K, the effectiveness factors, η , defined as the ratio between the overall rate of reaction and the rate of gasification if no mass transfer limitations were present within the particle, were below 0.8, indicating that the effect of internal mass transfer becomes increasingly significant at temperatures above 1173 K.

3.4. External mass transfer

It is assumed that if small particles of char are added to a fluidised bed they enter the particulate phase, being roughly of the same order of size and mass as the sand, and are then subject to the interstitial gas velocity through the particulate phase. Hence, the Reynolds number for flow of the particulate phase gas around the particles is small, leading to the common assumption of a spherically symmetrical mass transfer boundary layer [58].

The material balance for the boundary layer around the particle of char, *i.e.* from $r = R_p$ to $r = R_p + \delta$, under pseudo-steady state conditions for the i -th species leads to

$$\frac{1}{r^2} \frac{d(r^2 J_i)}{dr} - \xi_i = 0. \quad (10)$$

Here, J_i is the molar flux per unit area of species i and ξ_i is the molar rate of production of species i based on volume unit of bed. For combustion in air i is one of N_2 , O_2 , CO_2 , CO , whilst for oxy-firing N_2 can be excluded [32]. Equation (10) was rearranged to give Equations (11) to (14). It was assumed that ξ_i was zero for all species, *i.e.* there are no secondary reactions within the mass transfer boundary layer, δ .

$$\frac{dJ_{CO}}{dr} = \xi_{CO} - \frac{2}{r} J_{CO} \quad (11)$$

$$\frac{dJ_{CO_2}}{dr} = \xi_{CO_2} - \frac{2}{r} J_{CO_2} \quad (12)$$

$$\frac{dJ_{N_2}}{dr} = \xi_{N_2} - \frac{2}{r} J_{N_2} \quad (13)$$

$$\frac{dJ_{O_2}}{dr} = \xi_{O_2} - \frac{2}{r} J_{O_2} \quad (14)$$

The molar fluxes in the boundary layer are given by the Stefan-Maxwell equations ([32],[57]):

$$\frac{dy_{CO}}{dr} = \frac{RT}{P} \left\{ \frac{y_{CO} J_{N_2} - y_{N_2} J_{CO}}{D_{CO,N_2}^{eff}} + \frac{y_{CO} J_{CO_2} - y_{CO_2} J_{CO}}{D_{CO,CO_2}^{eff}} + \frac{y_{CO} J_{O_2} - y_{O_2} J_{CO}}{D_{CO,O_2}^{eff}} \right\} \quad (15)$$

$$\frac{dy_{CO_2}}{dr} = \frac{RT}{P} \left\{ \frac{y_{CO_2} J_{N_2} - y_{N_2} J_{CO_2}}{D_{CO_2,N_2}^{eff}} + \frac{y_{CO_2} J_{CO} - y_{CO} J_{CO_2}}{D_{CO_2,CO}^{eff}} + \frac{y_{CO_2} J_{O_2} - y_{O_2} J_{CO_2}}{D_{CO_2,O_2}^{eff}} \right\} \quad (16)$$

$$\frac{dy_{N_2}}{dr} = \frac{RT}{P} \left\{ \frac{y_{N_2}J_{CO_2} - y_{CO_2}J_{N_2}}{D_{N_2,CO_2}^{eff}} + \frac{y_{N_2}J_{CO} - y_{CO}J_{N_2}}{D_{N_2,CO}^{eff}} + \frac{y_{N_2}J_{O_2} - y_{O_2}J_{N_2}}{D_{N_2,O_2}^{eff}} \right\} \quad (17)$$

$$\frac{dy_{O_2}}{dr} = \frac{RT}{P} \left\{ \frac{y_{O_2}J_{CO_2} - y_{CO_2}J_{O_2}}{D_{O_2,CO_2}^{eff}} + \frac{y_{O_2}J_{CO} - y_{CO}J_{O_2}}{D_{O_2,CO}^{eff}} + \frac{y_{O_2}J_{N_2} - y_{N_2}J_{O_2}}{D_{O_2,N_2}^{eff}} \right\} \quad (18).$$

where y_i is the mole fraction of species i . Strictly speaking, with non-equi-mass diffusion, a pressure gradient is required to ensure conservation of momentum; however, in all experiments presented in this paper, the permeability of the bed is large, and pressure gradients small compared to the absolute pressure and that required to ensure fluidisation. Thus, pressure variations can be neglected in this model, and the pressure is taken to be constant.

The effective diffusion coefficient, $D_{i,j}^{eff}$, is given by

$$D_{i,j}^{eff} = \frac{\varepsilon D_{i,j}}{\tau^2} \quad (19)$$

where the molecular diffusivities, $D_{i,j}$, were calculated using the equation of Fuller *et al.* [59]; ε is the voidage in the particulate phase and τ^2 , the tortuosity, corrects for the fact that some area for flow is occupied by fluidised particles, and that the diffusion path is lengthened by gas having to diffuse around these particles. For the diffusion of N species, only $(N-1)$ of the Stefan-Maxwell equations are independent. Furthermore, the continuum diffusion coefficients were used since the spaces between particles in the particulate phase have lengths scales $d_a = 390 \mu\text{m}$, much greater than the mean free path for the gas molecules.

Solving the set of Equations (11) to (18), for each of the species involved is complicated by the fact that the complete set of boundary conditions is not known either at the surface of the particle ($r = R_p$) or at the boundary with the bulk flow ($r = R_p + \delta$). The mole fractions at $r = R_p + \delta$ are straightforwardly set by the mixture of gases fed into the reactor. At the surface of the particle, the assumption has been made that the combustion is controlled by external mass transfer of O_2 , giving $y_{O_2,s} = 0$ (discussed in Section 5.2.) Thus, the boundary conditions for all air and oxy-fuel combustion experiments were:

$$r = R_p \quad y_{O_2,s} = 0 \quad (20)$$

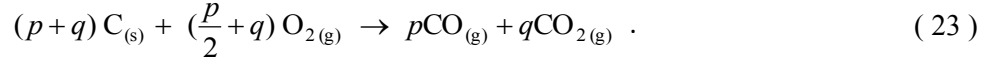
$$r = R_p + \delta \quad y_i = y_{i,bulk}, \text{ where } i = O_2, N_2, CO_2, CO. \quad (21)$$

Since N_2 is inert, $J_{N_2} = 0$ at the surface of the particle (and indeed everywhere). An important parameter in the solution of the mass transfer equations surrounding the particle is the thickness of the boundary layer, δ , surrounding the spherical particle of char. The determination of this parameter is described in Appendix A.

Finally, conservation of carbon and oxygen atoms at the surface of the particle yields conditions for the molar fluxes. In terms of molar fluxes, conservation of O_2 yields:

$$2J_{O_2} + J_{CO} + 2J_{CO_2} = 0. \quad (22)$$

Now, considering the global chemical equation for oxidation of carbon at the external surface of the particle:



In the simple case without gasification, the total flux of carbon leaving the particle (equal to the rate of combustion per unit external surface area) is

$$J_{CO} + J_{CO_2} = -\frac{p+q}{p/2+q}J_{O_2} = -\frac{p/q+1}{p/(2q)+1}J_{O_2} \quad (24)$$

where $p/q = \gamma$ and $\gamma = 2500\exp[-6240/T]$ from Eq. (5).

If the gasification reaction (3) is to be considered, the apparent gasification rate expressed as flux, R_g'' , in $\text{mol m}^{-2} \text{s}^{-1}$,

$$R_g'' = R'_g \frac{d_p \rho_e}{6} \quad (25)$$

must be added to Eq. (24), for char particles with an initial density, ρ_e and apparent diameter, d_p .

The total flux of elemental carbon away from the surface is now given by

$$J_{CO} + J_{CO_2} = -\frac{p/q+1}{p/(2q)+1}J_{O_2} + \frac{R_g''}{2} \quad (26)$$

Finally Eq. (26) can be combined with Eq. (22) to give J_{CO} and J_{O_2} in terms of J_{CO_2} :

$$J_{CO} = \frac{(B-1)J_{CO_2} + 0.5R_g''}{(1-B/2)} \quad (27)$$

$$J_{O_2} = -\left[\frac{J_{CO_2} + 0.5R_g''}{(1-B/2)} \right] \quad (28)$$

where $B = \frac{p+q}{p/2+q} = \frac{\gamma+1}{\gamma/2+1}$.

A pseudo time-marching scheme was used to solve the model equations. This involved guessing a complete set of variables at the surface of the particle ($r = R_p$) and stepping outwards to the edge of the boundary layer ($r = R_p + \delta$) using a differential equation solver. It was then possible to adjust the initial guesses until the free stream boundary conditions were met. This was done using Matlab's inbuilt ODE solver, *ode45*, which uses a Runge-Kutta method.

Using Eqs. (11) to (18), the first derivatives of the mass fractions and the molar fluxes can be calculated at any point in space given the mole fractions and the molar fluxes themselves. The variables are combined into one vector, herein defined as θ , so that $d\theta/dr$ incorporates all the derivatives:

$$\boldsymbol{\theta} = [J_{\text{CO}} \quad J_{\text{CO}_2} \quad J_{\text{N}_2} \quad J_{\text{O}_2} \quad y_{\text{CO}} \quad y_{\text{CO}_2} \quad y_{\text{N}_2} \quad y_{\text{O}_2}] \quad (29)$$

$$\frac{d\boldsymbol{\theta}}{dr} = \left[\frac{dJ_{\text{CO}}}{dr} \quad \frac{dJ_{\text{CO}_2}}{dr} \quad \frac{dJ_{\text{N}_2}}{dr} \quad \frac{dJ_{\text{O}_2}}{dr} \quad \frac{dy_{\text{CO}}}{dr} \quad \frac{dy_{\text{CO}_2}}{dr} \quad \frac{dy_{\text{N}_2}}{dr} \quad \frac{dy_{\text{O}_2}}{dr} \right]. \quad (30)$$

In an outer loop Matlab's *fsolve* routine was used to vary the 'free' initial conditions (*i.e.* the mole fractions of N₂, CO and CO₂ and the molar flux of CO₂, J_{CO_2} , at the surface of the particle) until the error between the computed and specified free stream boundary conditions was below a specified tolerance.

4. Results

4.1. Variation of initial rate with batch mass

Figure 3 shows the typical measured change in the mole fraction of O₂ across the bed, $\Delta(y_{\text{O}_2}) = y_{\text{O}_2, \text{out}} - y_{\text{O}_2, \text{in}}$, during the combustion of a batch of lignite char at 1023 K in air. The graph shows a maximum consumption of O₂ at $t \approx 0$; after this, $\Delta(y_{\text{O}_2})$ decreases until the reaction finishes after about 60 s. The overall rate of carbon conversion, R'_c , in $\text{mmol s}^{-1} \text{g}^{-1}$, was calculated from the change in oxygen concentration across the bed using Eq. (31), where \dot{N} is the total molar flow rate of gas through the bed (assumed constant) and m_{batch} is the initial mass of the batch of char.

$$R'_c = \frac{\dot{N} \Delta(y_{\text{O}_2})}{m_{\text{batch}}} \quad (31)$$

[Figure 3 hereabouts]

An optimal mass of batch, m_{batch} , for the experiments had to be ascertained to ensure that it was neither large enough for the transfer of gas from the bubble phase to the particulate phase to control or influence the rate of combustion nor so small as to render actual deviations in the concentrations in the off-gas being influenced substantially by experimental noise. This was verified by performing experiments in which progressively larger batches of lignite char with masses between 0.05 and 0.47 g (and mass intervals of ~ 0.03 g), were added to a bed fluidised in air at 1023 K. Figure 4 shows that, for batches between 0.05 and 0.30 g, the average initial rate of carbon conversion, $R'_{c,0}$, was $\sim 2.29 \pm 0.07 \text{ mmol s}^{-1} \text{g}^{-1}$ indicating that, for batches in this range of mass, cross flow between the bubble and the particulate phases did not limit the reaction. For m_{batch} larger than ~ 0.30 g, $R'_{c,0}$ decreased almost linearly by further increasing the batch mass. Thus, all experiments described in the following sections were performed with $m_{\text{batch}} \sim 0.25$ g. The relatively large batch maximised the

deviation between the inlet and outlet concentrations of O₂, thereby reducing the error associated with calculating rates of reaction, which use difference in [O₂] between inlet and outlet.

[Figure 4 hereabouts]

The rate of carbon conversion, X , over time was, in turn, defined as

$$\frac{dX}{dt} = \frac{12\dot{N}\Delta(y_{O_2})}{m_{batch}\varphi} = \frac{12R'_c}{\varphi}. \quad (32)$$

Here, φ is the mass fraction of carbon in the char, equal to 0.8569 from Table 1. Figure 5(a) shows the total carbon conversion, as calculated from Eq. (32), for the 15 batches described in Figure 4. The average conversion for all experiments was $\sim 1.0 \pm 0.013$, indicating a good closure of the mass balance and accurate readings of the mole fraction of O₂ with the UEGO sensor. Figure 5(b) shows the conversion of carbon with time for 6 different batch masses. The similar transient conversion profiles for the batches with mass ≤ 0.29 g confirm the observations from Figure 4 to find an optimum value for m_{batch} .

[Figure 5 hereabouts]

4.2. Effect of particle diameter on the combustion of lignite char

A series of experiments was performed for a variety of char particle sizes, *i.e.* average d_p of 655, 780, 1200, 1550, 2030 and 2580 μm , across a range of temperatures from 1023 to 1223 K. Figure 6 shows the initial rates, $R'_{c,0}$, against d_p for several batches at different temperatures. It can be seen that (i) the rates vary very little with temperature, particularly with larger char particle sizes, *i.e.* $d_p \geq 1200 \mu\text{m}$, and (ii) there is a clear dependence of the rates on particle diameter. Taking (i) and (ii) together suggests that combustion is controlled by external mass transfer to the particle. Any slight temperature dependence of the rates can be attributed to changes in the diffusivities of the gases. Hence, for the experiments described in Section 4.3, it was decided to use char particles with an average diameter of 1200 μm .

[Figure 6 hereabouts]

4.3. Rates of combustion in air compared with oxy-fuel

Batch experiments with lignite char were undertaken under oxy-fuel conditions in 20.9 mol.% O₂, balance CO₂, for temperatures between 1023 and 1223 K. The initial rates, assuming a total carbon conversion to CO₂, are shown in Figure 7 and compared with the equivalent initial rates measured during air combustion (20.9 mol.% O₂, balance N₂). The rate for the oxy-fuel experiments increases considerably with temperature. At low temperatures, *i.e.* below 1123 K, the overall rate of carbon conversion was lower under oxy-fuel conditions than for air combustion, as noted above for 1023 K. At $T \sim 1123$ K, the rate was very similar in both cases and, at higher temperatures, oxy-fuel rates were faster than air combustion rates.

[Figure 7 hereabouts]

Experiments were also undertaken with an inlet mole fraction of O₂ of 2.5 mol.%, balance N₂ or CO₂. The observed initial rates of carbon conversion at different temperatures are shown in Figure 8. Again, there appeared to be little temperature dependence on $R'_{c,0}$ for combustion with diluted air. At $T \geq 1073$ K, the observed rates in oxy-fuel were significantly faster than in diluted air.

[Figure 8 hereabouts]

Figure 9 shows the profiles of the overall rate of carbon conversion over time for two different temperatures under air and oxy-fuel combustion with $y_{O_2, bulk}$ of (a) 20.9 and (b) 2.5 mol.%, balance N₂ or CO₂ for air and oxy-fuel combustion, respectively. Interestingly, the conversion of carbon was faster for air than for oxy-fuel combustion at 1023 K. However, at 1223 K, the conversion of oxy-fuel combustion was faster, particularly with $y_{O_2, bulk} = 0.025$ (Figure 9(b)), where the total burnout time is reduced by ~ 280 s (and only by ~ 5 s with $y_{O_2, bulk} = 0.209$).

[Figure 9 hereabouts]

5. Discussion

5.1. Particle temperatures

The experiments summarised in Figure 7 suggest that there is an increase in the overall rate of carbon conversion with temperature during oxy-fuel combustion owing to rates of gasification becoming significant, particularly at $T \geq 1123$ K. However, it is expected that Reaction (2) and the oxidation of CO sufficiently close to the particle, Reaction (4), both being highly exothermic, would lead to an increase in the temperature of the particle of char. A significant change in the temperature of the particle could have some effect on the rate of carbon conversion, particularly under oxy-fuel conditions, as gasification is rather sensitive to temperature under the conditions studied. Thus, in order to determine the average difference in temperature between a particle of char and the fluidised bed, a steady-state energy balance on a reacting particle was performed [60], thus:

$$-R_c''[(1-\chi_2)(\Delta H_1 + \chi_1(\Delta H_2 - \Delta H_1)) + \chi_2\Delta H_3] = \pi d_p^2 h(T_p - T_b) + \varepsilon_r \pi d_p^2 \sigma(T_p^4 - T_b^4) \quad (33)$$

where R_c'' is the rate of carbon conversion of a single particle of char in mol s⁻¹, *i.e.* $R_c'' = R'_{c,0}(V_p \rho_e)$; χ_1 is the fraction of the carbon, which oxidises to CO₂ sufficiently close to the particle of char to transfer all its heat of reaction to the particle, here taken as $\chi_1 = 1/(1 + \gamma)$; χ_2 is the fraction of the carbon, which oxidises to CO *via* Reaction (3), *i.e.* $\chi_2 = (0.5 \times R'_g)/R'_c$. In Eq. (33), h is the heat transfer coefficient from the particle to the bed, here assumed to be in the range 500 ± 150 W m⁻² K⁻¹, in accordance with reported values from several different methods for $d_p \sim 1200$ μ m and $d_a \sim 390$ μ m [64]; ε_r is the emissivity of the particle, taken to be unity [60]; σ is the Stefan-Boltzmann constant (5.67×10^{-8} W m⁻² K⁻⁴); T_p is the temperature of the particle and T_b is the temperature of the bed.

Care is needed when using Eq. (33) in the model to avoid a circular argument. First, the initial rates of gasification and carbon conversion ($R'_{g,0}$ and $R'_{c,0}$, respectively) are estimated by using the temperature of the bed, T_b , which are in turn used to estimate the temperature of the particle, T_p , from Eq. (33). Then, the initial reaction rates are recalculated using T_p as the temperature of reaction. Typically, $T_p > T_b$, thus the new estimate of the rate of gasification would be higher than the original estimate and a lower T_p is expected than that initially calculated owing, mainly, to the endothermic gasification reaction. Hence, the new rate of reaction is used to calculate a new T_p in an iterative process until $|R'_g(i) - R'_g(i-1)| \leq 1 \times 10^{-10}$, where i is the number of iterations performed.

5.2. Solution of the model

The model was initially investigated by using the kinetic results from [35], shown in Table 2, for the gasification of lignite char at 1173 K, and Eq. (5) for the combustion ratio CO:CO₂. Figure 10 shows (a) the mole fraction profile and (b) molar fluxes of CO, CO₂ and O₂ within the boundary layer thickness for combustion in air. Here σ_r is the dimensionless radius in the external boundary later defined as $\sigma_r = r/R_p$. Also plotted, for reference, is the combustion in air with the rate of gasification, $R'_{g,0}$, taken to be zero. It is clear that, in this case, the gasification reaction makes very little difference to the flux of carbon leaving the combusting particle. This is expected as the [CO₂] is very low at the surface of the particle compared to the much larger [CO]. The initial overall rate of carbon conversion predicted with the model was $R'_{c,0} = 2.63 \text{ mmol g}^{-1} \text{ s}^{-1}$, with the gasification rate, $R'_{g,0}$, contributing only $\sim 0.13 \text{ mmol g}^{-1} \text{ s}^{-1}$. The estimated temperature difference between the particle and the bed, $\Delta T = T_p - T_b$, was 55 K.

[Figure 10 hereabouts]

Figure 11 shows the equivalent results but under oxy-fuel conditions. In this case, the inclusion of the gasification reaction has a significant effect on the overall reaction, and thus on the mole fractions and fluxes close to the surface of the char. The initial overall rate of carbon conversion predicted with the model was $R'_{c,0} = 2.88 \text{ mmol g}^{-1} \text{ s}^{-1}$, with gasification rate, $R'_{g,0} \sim 0.85 \text{ mmol g}^{-1} \text{ s}^{-1}$. The estimated ΔT was 41 K. Ignoring the gasification rate under these conditions (dotted lines in Figure 11) would decrease the overall predicated rate by $\sim 27\%$. Of course this is only true at temperatures high enough for the gasification rate to be significant, *i.e.* $T \geq 1123 \text{ K}$ for lignite char [6],[35]. At lower temperatures, say 1073 K, the gasification rate is much slower and has little effect on the overall rate of carbon conversion under oxy-fuel conditions. For example under the same conditions as in Figure 11 but at 1073 K the model gave $R'_{c,0} = 1.93 \text{ mmol g}^{-1} \text{ s}^{-1}$, with $R'_{g,0} = 0.07 \text{ mmol g}^{-1} \text{ s}^{-1}$.

[Figure 11 hereabouts]

Figure 12(a) shows the predicted initial overall rates of conversion of carbon for combustion in air at different bed temperatures and for char particles of different sizes. These results were compared with the average rates observed experimentally under the same conditions (shown in Figure 6). For

particles with $d_p \geq 1200 \mu\text{m}$, there is a remarkable agreement between the predicted and the measured rates, validating the underlying physics and assumptions used in the model. The model also predicted a negligible temperature dependence on the rates of air combustion between 1023 and 1223 K. However, with small char particle sizes, *i.e.* $d_p < 1000 \mu\text{m}$, the model tends to over-predict the rates of combustion, especially at higher temperatures, *i.e.* $T \geq 1123 \text{ K}$; there appeared to be a slightly higher dependence. The contribution of the gasification reaction for all cases in Figure 12(a) was $< 3\%$ of the overall rate of carbon conversion. Figure 12(b) shows the estimated temperature rise between the particle and bed, ΔT , using $h = 500 \text{ W m}^{-1} \text{ K}^{-1}$: ΔT was between ~ 30 and 60 K for particles with $d_p \geq 1200 \mu\text{m}$ and between ~ 75 and 100 K for smaller size particles. These values of ΔT are relatively small compared to experimental values reported in the literature for the combustion of large particles of carbon in beds fluidised by air, *e.g.* $\Delta T \sim 150 \text{ K}$ for $d_p = 6500 \mu\text{m}$ [60]. However, others ([55],[60]) have also concluded that small particles burn at a temperature close to that of the bed because of the high heat transfer coefficient for small particles. The fact that the gas used in this work was dry could also explain the relative low temperature rise of the char particles compared to the higher temperatures usually observed when water vapour is present in the mixture [61] due to, largely, oxidation of CO by H₂O. In Figure 12(b) ΔT increases as d_p decreases since the same value of h was used for all particle sizes. However, increasing the value of h for the smallest particles, *i.e.* $d_p = 655$ and $780 \mu\text{m}$, would have little effect on $R'_{c,0}$ for air combustion due to the small temperature dependence predicted for these particle sizes. Accounting for the contribution of the temperature rise of the particle increased the combustion rate, $R'_{c,0}$, by an average of $3.3 \pm 1.7\%$.

[Figure 12 hereabouts]

In Sections 3.3 and 3.4 it was assumed that oxygen does not diffuse into the centre of the particle because it reacts immediately on the external surface, *i.e.* $y_{\text{O}_2,s} = 0$. To test this assumption, the modelled molar fluxes of O₂ at the surface of the particle, $J_{\text{O}_2,s}$, were compared with the rates of carbon conversion observed experimentally. Assuming that most of the carbon reacting at the surface of the burning particle reacts to CO (Reactions (1) and (3)), the estimated flux of carbon leaving the particle, *i.e.* $(-2 \times J_{\text{O}_2,s})$, was, for all cases investigated in this work for air combustion, very close to the initial observed rates of carbon conversion, $R'_{c,0(\text{exp})}$. For example, at 1173 K , $d_p = 1200 \mu\text{m}$ and $y_{\text{O}_2,\text{bulk}} = 0.209$, $R'_{c,0(\text{exp})} = 0.474 \text{ mol m}^{-2} \text{ s}^{-1}$ and $(-2 \times J_{\text{O}_2,s}) = 0.465 \text{ mol m}^{-2} \text{ s}^{-1}$. Under the same conditions but with $y_{\text{O}_2,\text{bulk}} = 0.025$, the experimental and theoretical fluxes were, respectively, 0.054 and $0.058 \text{ mol m}^{-2} \text{ s}^{-1}$. These observations validate the assumption of the model that all (or most of) the oxygen reacts on the external surface.

5.3. Effect of gasification under air and oxy-fuel combustion at different compositions of O₂

The experiments presented in Section 4.3 were modelled to compare the initial overall rates of conversion between the observed and predicted initial rates of reaction. Figure 13(a) shows that the model predicts very accurately the observed rates at all temperatures between 1023 and 1223 K. By including the rate of gasification by CO₂ for the oxy-fuel case (Figure 13(b)), the model also predicts very accurate results, particularly between 1023 and 1173 K. However, at 1223 K, the model overestimates slightly the overall rate of reaction by predicting rates of gasification higher than those observed. This discrepancy could be owing to the fact that intra-particle mass transfer limitations for the gasification of lignite char were initially ignored in this model. It was suggested elsewhere [35] that for this type of lignite char the effectiveness factor within the particle of char, η , (defined as the ratio between the overall rate of reaction and the rate of gasification if no mass transfer limitations were present within the particle) was significant for temperatures above 1173 K, *e.g.* ~ 0.65 at $T = 1223$ K. Thus, the model was examined again using η to modify the rate of gasification, *i.e.* $R'_{g,0,overall} = R'_{g,0} \times \eta$, where η was obtained by fitting a curve to the effectiveness factors at different temperatures reported in [35]. This was applied to all cases when $T_p > 1173$ K. The new predicted values, indicated in Figure 13(b) with (○), are very similar to the observed rates indicating that intra-particle limitations cannot be ignored under oxy-fuel conditions at high temperatures, *i.e.* $T_p > 1173$ K and for highly reactive chars. Considering intra-particle limitations of the gasification reaction under air combustion conditions had negligible effect on $R'_{c,0}$ as the contribution of the gasification reaction is very small even at high temperatures, *e.g.* $0.002 < \chi_2 < 0.026$ for the model predictions shown in Figure 13(a).

Figure 13 suggests that, for char particles with diameter of the order of $\sim 1200 \mu\text{m}$ and $y_{\text{O}_2, \text{bulk}} = 0.209$, the overall rate of conversion of carbon with oxy-fuel shows a rather larger dependence on temperature than does combustion in air, owing to the significance of the gasification reaction which is not so limited by external mass transfer. One consequence of this is that above ~ 1123 K the overall rate in the oxy-fuel case becomes faster than that in air. There is, of course, a separate effect caused by the different diffusivities of O₂ in CO₂ and N₂ but it is believed to be secondary at temperatures where gasification rates are high, as discussed later in Section 5.4. The average temperature rise estimated with the model (with $h = 500 \text{ W m}^{-2} \text{ K}^{-1}$) was 58 ± 4 K for air-firing combustion and 45 ± 8 K for the oxy-fuel case, with the lower values of ΔT as the bed temperature increases due to (i) higher rates of gasification, and (ii) less formation of CO₂ at the surface of the particle. With $h = 350 \text{ W m}^{-1} \text{ K}^{-1}$, ΔT s were about 9 to 12 K higher than the average values with $h = 500 \text{ W m}^{-1} \text{ K}^{-1}$ while with $h = 650 \text{ W m}^{-1} \text{ K}^{-1}$ ΔT s were about 6 to 8 K lower. The effect of these small variations in T_p owing to the different heat transfer coefficients had little effect on the overall rate of carbon conversion, with variations of $R'_{c,0}$ within 1 and 3.5% for air and oxy-fuel combustion,

respectively. Furthermore, ignoring completely any changes in the temperature of the particle, *i.e.* Eq. (33), had also little effect on the predicted rates of carbon conversion for air combustion, *viz.* less than 5% deviation from the results shown in Figure 13(a). However, for the oxy-fuel case, the predictions of $R'_{c,0}$ would have been between 4% and 20% lower than the values in Figure 13(b). Thus, changes in the temperature of the particle could have a significant effect on oxy-fuel combustion owing to the sensitivity of the gasification reaction with temperature, particularly at $T_p \geq 1173$ K, when gasification rates are significant with this type of char.

[Figure 13 hereabouts]

Figure 14(a) shows good agreement between the model and the experimental results for the combustion of char in 2.5 mol% O₂, balance N₂. Under oxy-fuel conditions, Figure 14(b) also shows good agreement between experiment and model for $T_b \leq 1173$ K. However, at $T_b = 1223$ K, the model overestimates the overall rate of reaction by about 25% if intra-particle mass transfer limitations are ignored. Of course, with $y_{O_2,bulk} = 2.5$ mol.%, the apparent rate of gasification is much more significant than with 20.9 mol.% due to the much higher [CO₂] in the fluidising gas. The average temperature rise estimated with the model (with $h = 500 \pm 150$ W m⁻¹ K⁻¹) was only about 7 ± 2 K for air-firing combustion (Figure 14(a)). For the oxy-fuel case, (Figure 14(b)), ΔT was between 6 ± 2 K at $T_b = 1023$ K and -2 ± 1 K at $T_b = 1223$ K. Thus, under these experimental conditions, the char particles burnt at a temperature very close to that of the bed and the effect of the small variations in T_p had little effect on the predicted values of $R'_{c,0}$. In this case, intra-particle mass transfer limitations were examined with the model only for the case of $T_b = 1223$ K in Figure 14(b): at $T_b = 1173$ K the temperature of the particle was found to be the same as that of the bed. The new predicted value, indicated in Figure 14(b) with (○), is very similar to the observed rate. Furthermore, with $y_{O_2,bulk} = 2.5$ mol.%, the overall rate of oxy-fuel combustion becomes faster than for air combustion at temperatures as low as 1073 K.

[Figure 14 hereabouts]

Comparing the two cases described above with $y_{O_2,bulk} = 2.5$ and 20.9 mol.%, it appears that the temperature at which oxy-fuel combustion becomes faster than combustion in air (or diluted air) is dependent on the mole fraction of O₂ and thus the corresponding balance of N₂ or CO₂. Under mass transfer control, the rate of reaction with O₂ depends on the driving force for oxygen diffusion (*i.e.* $y_{O_2,bulk}$) through the boundary layer. In contrast, under oxy-fuel conditions, the rate of gasification

might be expected to be relatively insensitive to $y_{O_2,bulk}$, since the gas close to the surface of the combusting particle should be largely CO_2 . Thus, at small mole fractions of O_2 , gasification could account for a larger proportion of the total carbon conversion rate. Figure 15 shows the rates calculated from the model with bulk mole fractions of O_2 between 5 and 20 mol% with balance N_2 or CO_2 . The temperature of the bed chosen for this comparison was, deliberately, 1123 K. At this temperature, gasification rates with lignite char are high enough to be significant under oxy-fuel conditions but not enough to be significantly affected by intra-particle mass transfer. The mole fraction of CO at the surface of the particle, $y_{CO}(\sigma_r = 1)$ shown in Figure 15(a), was much higher in oxy-fuel than in air combustion, with a slightly larger difference between the two cases at lower values of $y_{O_2,bulk}$ owing to the higher gasification rates with oxy-fuel. Figure 15(b) shows that with low $y_{O_2,bulk}$ the gasification rate accounted for almost 23% of the overall rate under oxy-fuel conditions while being less than 10% when $y_{O_2,bulk} = 0.20$. Under air combustion, the gasification rate accounted for less than 3% for all values of $y_{O_2,bulk}$ investigated. At 1123 K, the overall rates of carbon conversion with oxy-fuel are slightly higher with $y_{O_2,bulk} \leq 0.05$. The rates become practically equal with $y_{O_2,bulk} = 0.10$ and with larger $y_{O_2,bulk}$ air combustion becomes slightly faster than oxy-fuel combustion despite [CO] at the surface is still higher for the latter case. At this point, the difference in the diffusivities of O_2 in N_2 and CO_2 could be the main influence on the overall rate so that oxy-fuel combustion only becomes faster than air combustion at higher temperatures. Similar findings than the ones reported here on the significance of gasification during oxy-fuel combustion and the effect of $[O_2]$ in the inlet gas have been reported in the literature using different ranks of coals and reaction conditions. However, a large amount of this work has been reported in pf combustion (e.g. [61]-[63]) with less work on FBC (e.g.[33]).

[Figure 15 hereabouts]

5.4. Effect of diffusivities of O_2 in N_2 and CO_2

In order to investigate the effect of the diffusivities of O_2 in N_2 and CO_2 , the model was evaluated with different inlet mole fractions of O_2 under air combustion and oxy-fuel conditions and ignoring Reaction (3), i.e. setting $R'_g = 0$. Changes in the temperature of the particle were deliberately ignored so that the only variable at each temperature and $y_{O_2,bulk}$ was the balance gas, i.e. N_2 or CO_2 . The predicted initial rates of carbon conversion are shown in Figure 16. For all $y_{O_2,bulk}$ and

temperatures investigated, $R'_{c,0}$ was larger when the balance gas was N_2 than when exchanged for CO_2 . The average ratio of the initial rates of air combustion over oxy-fuel combustion, *i.e.* $R'_{c,0(\text{combustion})} / R'_{c,0(\text{oxy-fuel})}$, was for all five temperatures *ca.* 1.17, 1.21 and 1.23 with $y_{O_2,bulk} = 20.9$, 10.0 and 2.5 mol.%, respectively. These results confirm that, at low temperatures (*e.g.* 1023 K), the smaller initial reaction rates of lignite char at identical $[O_2]$ in an O_2/CO_2 atmosphere compared to O_2/N_2 mixtures are due to the lower binary diffusivity of O_2 in CO_2 than that in N_2 . At higher temperatures (*e.g.* 1223 K) the higher initial rates observed and predicted under oxy-fuel conditions compared with air combustion, *e.g.* Figures 13 and 14, are due to the more significant reaction rates of gasification, without which $R'_{c,0}$ would be somewhat lower for the former than for the latter case.

[Figure 16 hereabouts]

6. Conclusions

The rate of combustion of lignite char in air and oxy-fuel was measured experimentally in a fluidised bed for a range of temperatures between 1023 and 1223 K. A useful component of the experimental apparatus was the UEGO sensor, which enabled very rapid measurements of the oxygen partial pressure in the off-gas. It was shown that the sensor operated as if it were a total combustion meter, measuring the concentration of O_2 which would result if all the char were to burn to CO_2 . Carbon balances for the batches of char were, for most cases, above 95%, indicating accurate measurements of the oxygen partial pressures and justifying the use of this sensor for this type of application. For combustion in air the reaction was found to be externally mass-transfer limited, based on there being little temperature dependence of the overall rate of conversion. At low temperatures, *e.g.* 1023 K, initial reaction rates of lignite char at identical $[O_2]$ were found to be smaller in an O_2/CO_2 atmosphere compared to O_2/N_2 mixtures and corresponding burnout times were longer in oxy-fuel. These differences were explained by the lower diffusivity of gaseous components when immersed in an enriched CO_2 atmosphere. However, at high temperatures, *e.g.* 1223 K, initial reaction rates of lignite char at identical concentrations of O_2 were found to be larger in an oxy-fuel atmosphere compared to those in mixtures of oxygen and nitrogen. Burnout times were, respectively, shorter for the former than for the latter case. This was attributed to the more significant rates of gasification of carbon with CO_2 under oxy-fuel conditions at high temperatures. The point at which oxy-fuel rates become more significant than those in air depends not only on temperature, char particle size, and coal rank (the latter two not investigated in this work), but also on the concentration of O_2 in the fluidising gas, *e.g.* $T \sim 1023$ K with $y_{O_2,bulk} = 0.025$ and $T \sim 1123$ K with $y_{O_2,bulk} = 0.209$.

A mathematical model coupling the intrinsic kinetics of the gasification and combustion of lignite char with the mass transfer limitations surrounding the particle of char was developed. Differences in the temperature between the particle and the bed were estimated and found to be $\sim 58 \pm 4$ K for air-firing combustion and 45 ± 8 K for oxy-fuel when $y_{O_2,bulk} = 0.209$. This rise of the temperature of the particle had a significant effect for the model predictions with oxy-fuel but was almost negligible for air combustion. With $y_{O_2,bulk} = 0.025$, the particles of carbon were found to burn very close to the temperature of the bed. There was excellent agreement between the modelled and observed rates of carbon conversion at $T_p \leq 1173$ K. At higher temperatures, the model overestimated the results if no intra-particle mass transfer was considered for the gasification reaction. The model further supported the notion that the gasification reaction at the surface is responsible for the non-zero activation energy for oxy-fuel combustion and that the combustion reaction is largely unaffected except in so far as the concentrations at the surface change. Finally, the good agreement between the predicted and the observed rates suggest that oxidation of CO occurs well away from the particle as the oxy-fuel rates were found to be sensitive to changes in the temperature of the particle.

Acknowledgements

The authors would like to thank Kieran Hegarty and Toyin Omojola from the Department of Engineering, Cambridge University. Financial support from the Engineering and Physical Sciences Research Council (Grant reference number: EP/G063265/1) and the Consejo Nacional de Ciencia y Tecnología (CONACYT) is also acknowledged.

References

- [1] BP Sustainability Reporting 2011. *BP and Sustainability*. [online] Available at: <http://www.bp.com/sectiongenericarticle800.do?categoryId=9036316&contentId=7067089> [Accessed 23 November 2012].
- [2] International Energy Agency. Key World Energy Statistics. Paris: OECD IEA 2012.
- [3] Sims REH, Schock RN, Adegbulugbe A, Fenhann J, Konstantinaviciute I, Moomaw W, Nimir HB, Schlamadinger B, Torres-Martínez J, Turner C, Uchiyama Y, Vuori SJV, Wamukonya N, Zhang X. 2007: Energy supply. In *Climate Change 2007: Mitigation. Contribution of Working Group III to the Fourth Assessment Report of the Intergovernmental Panel on Climate Change* [Metz B, Davidson OR, Bosch PR, Dave R, Meyer LA (eds)], Cambridge University Press, Cambridge, United Kingdom and New York, NY, USA.
- [4] Edge P, Gharebaghi M, Irons R, Porter R, Porter RTJ, Pourkashanian M, Smith D, Stephenson P, Williams A. Combustion modelling opportunities and challenges for oxy-coal carbon capture technology. *Chem Eng Res Des* 2011; 89:1470–93.
- [5] Wall T, Liu Y, Spero C, Elliott L, Khare S, Rathnam R, Zeenathal F, Moghtaderi B, Buhre B, Sheng C, Gupta R, Yamada T, Makino K, Yu J. An overview on oxyfuel coal combustion — state of the art research and technology development. *Chem Eng Res Des* 2009;87(8):1003-16.
- [6] Dennis JS, Scott SA. In situ gasification of a lignite coal and CO₂ separation using chemical looping with a Cu-based oxygen carrier. *Fuel* 2010;89:1623-40.
- [7] Li YH, Lu GQ, Rudolph V. The kinetics of NO and N₂O reduction over coal chars in fluidised-bed combustion. *Chem Eng Sci* 1998;53:1-26.
- [8] Okawa M, Kimura N, Kiga T, Takano S, Arai K, Kato, M. Trial design for a CO₂ recovery power plant by burning pulverized coal in O₂/CO₂. *Energy Conversion and Management* 1997;38:S123-S127.
- [9] Kiga T. 2001. O₂/RFG combustion-applied pulverised coal fired plant for CO₂ recovery. In: Miura, T. (Ed.), *Advanced Coal Combustion*. Nova Science Publishers Inc., New York, pp. 185–241.
- [10] Jordal K, Anheden M, Yan J, Strömberg L. 2004. Oxyfuel combustion for coal-fired power generation with CO₂ capture – opportunities and challenges. In: *Proc. of 7th International Conference on Greenhouse Gas Technologies*, Vancouver, Canada.
- [11] Allam RJ, White V, Panesar RS, Dillon D. 2005. Optimising the design of an oxyfuel-fired advanced supercritical PF boiler. In: Sakkestad, B.A. (Ed.), *Proc. of the 30th International Technical Conference on Coal Utilization & Fuel Systems*. Coal Technology: Yesterday–Today–Tomorrow. Coal Technology Association, Clearwater, FL, USA, April 17–21.
- [12] Buhre BJP, Elliott LK, Sheng CD, Gupta RP, Wall TF. Oxy-fuel combustion technology for coal-fired power generation. *Prog Energy Combust. Sci* 2005;31(4):283–307.

- [13] Croiset E, Douglas PL, Tan Y. 2005. Coal oxyfuel combustion: a review. In: Proc. of the 30th International Technical Conference on Coal Utilization & Fuel Systems—Clearwater Coal Conference, Clearwater, FL, USA.
- [14] Wall T. 2005. Fundamentals of oxy-fuel combustion. In: IEA GHG Inaugural Workshop of the Oxy-fuel Combustion Network, Cottbus, Germany, November 29–30.
- [15] Santos S, Haines M, Davison J. 2006. Challenges in the development of oxy-combustion technology for coal fired power plant. In: Sakkestad, B.A. (Ed.), Proc. of the 31st International Technical Conference on Coal Utilization & Fuel Systems. Coal Technology Association, Clearwater, FL, USA.
- [16] Wall TF. Combustion processes for carbon capture. *Proc Combust Inst* 2007;31: 31–47.
- [17] Toftegaard MB, Brix J, Jensen PA, Glarborg P, Jensen AD. Oxy-fuel combustion of solid fuels. *Prog Energy Combust Sci* 2010;36(5):581–625.
- [18] Anheden M, Burchhardt U, Ecke H, Faber R, Jidinger O, Giering R, Kass H, Lysk S, Ramström E, Yan J. Overview of Operational Experience and Results from Test Activities in Vattenfall's 30 MWth Oxyfuel Pilot Plant in Schwarze Pumpe. *Energy Procedia* 2011;4:941–50.
- [19] Czakiert T, Bis Z, Muskala W, Nowak W, Fuel conversion from oxyfuel combustion in a circulating fluidized bed. *Fuel Processing Technology* 2006;87:531–8.
- [20] Jia L, Tan Y, Wang C, Anthony EJ. Experimental study of oxyfuel combustion and sulphur capture in a mini-CFBC. *Energy & Fuels* 2007;21:3160–4
- [21] Pikkarainen T. Small scale fluidized bed experiments under oxygen combustion conditions. In: 2007 International Conference on Coal Science and Technology, Nottingham, UK, 2007.
- [22] Czakiert T, Karski S, Szetkier K, Markiewicz D, Mirek P, Andrzejczyk M, Nowak W. Operating Experience with a 0.1MWth oxyfuel-CFB test rig. In: 1st Oxyfuel Combustion Conference, Cottbus, Germany, 2009.
- [23] Eddings EG, Okerlund R, Bool LE. Pilot-scale evaluation of oxycoal firing in circulating fluidized bed and pulverized coal-fired test facilities. In: 1st Oxyfuel Combustion Conference, Cottbus, Germany, 2009.
- [24] Jia L, Tan Y, Anthony EJ. Emissions of SO₂ and NO_x during oxyfuel CFB combustion tests in a mini-circulating fluidized bed combustion reactor. *Energy & Fuels* 2010;24:910–5.
- [25] Krzywanski J, Czakiert T, Muskala W, Sekret R, Nowak W. Modeling of solid fuel combustion in oxygen-enriched atmosphere in circulating fluidized bed boiler. Part 2: numerical simulations of heat transfer and gaseous pollutant emissions associated with coal combustion in O₂/CO₂ and O₂/N₂ atmospheres enriched with oxygen under circulating fluidized bed conditions, *Fuel Processing Technology* 2010;91:364–8.
- [26] Scala F, Salatino P. Flue gas desulfurization under simulated oxyfiring fluidized bed combustion conditions: the influence of limestone attrition and fragmentation, *Chem Eng Sci* 2010;65:556–61.

- [27] Lupion M, Diego R, Loubeau L, Navarrete B. CIUDEN CCS Project: status of the CO₂ capture technology development plant in power generation. *Energy Procedia* 2011;4:5639–46.
- [28] Romeo LM, Díez LI, Guedea I, Bolea I, Lupiáñez C, González A, Pallarés J, Teruel E. Design and operation assessment of an oxyfuel fluidized bed combustor. *Experimental Thermal and Fluid Science* 2011;35:477–84.
- [29] Seddighi S, Pallarés D, Johnsson F, Varonen M, Hyytiäinen I, Ylä-Outinen V, Palonen M. Assessment of oxyfuel circulating fluidized bed boilers—modeling and experiments in a 5 MW pilot plant, 2nd IEA GHG International Oxyfuel Combustion Conference, 2011.
- [30] Tan Y, Jia L, Wu Y, Anthony EJ. Experiences and results on a 0.8MWth oxy-fuel operation pilot-scale circulating fluidized bed. *Applied Energy* 2012;92:343–7.
- [31] de Diego LF, de las Obras-Loscertales M, Rufas A, García-Labiano F, Gayán P, Abad A, Adánez J. Pollutant emissions in a bubbling fluidized bed combustor working in oxy-fuel operating conditions: effect of flue gas recirculation. *Applied Energy* 2013;102:860–7.
- [32] Scala F. Calculation of the mass transfer coefficient for the combustion of a carbon particle. *Combustion and Flame* 2010;157(1):137.142.
- [33] Scala F and Chirone R. Combustion of Single Coal Char Particles under Fluidized Bed Oxyfiring Conditions. *Industrial & Engineering Chemistry Research* 2010;49(21):11029-11036.
- [34] Brown TA, Dennis JS, Scott SA, Davidson JF, Hayhurst AN. Gasification and Chemical-Looping Combustion of a Lignite Char in a Fluidized Bed of Iron Oxide. *Energy Fuels* 2010;24:3034–48.
- [35] Saucedo MA, Lim JY, Dennis JS, Scott SA. CO₂-gasification of a lignite coal in the presence of an iron-based oxygen carrier for Chemical-Looping Combustion. *Fuel* 2014;127:186-201.
- [36] Ross IB, Davidson JF. The combustion of carbon particles in a fluidized bed. *Trans Inst Chem Eng* 1982;60:108-14.
- [37] Collings N, Hegarty K, Ramsander T. Steady-state modelling of the universal exhaust gas oxygen (UEGO) sensor. *Meas Sci Technol* 2012;23:085108.
- [38] Wen CY, Yu YH. A generalized method for predicting minimum fluidization velocity. *AIChE J* 1966;12(3):610–2.
- [39] Scala F, Chirone R. Combustion of single coal char particles under fluidized bed oxyfiring conditions. *Ind Eng Chem Res* 2010;49:11029-36.
- [40] Fennell PS, Dennis JS, Hayhurst AN. The order with respect to oxygen and the activation energy for the burning of an anthracitic char in O₂ in a fluidised bed, as measured using a rapid analyser for CO and CO₂. *Proceedings of the Combustion Institute* 2009;32:2051-8.
- [41] Regitz S, Collings N. Fast response air-to-fuel ratio measurements using a novel device based on a wide band lambda sensor. *Meas Sci Technol* 2008;19:075201.

- [42] Lee JH. Review on zirconia air-fuel ratio sensors for automotive applications. *J Math Sci* 2003;38:4247–57.
- [43] Yamada T, Hayakawa N, Kami Y, Kawai T. Universal air-fuel ratio heated exhaust gas oxygen sensor and further applications. *SAE Technical Paper Series* 1992;920234.
- [44] Regitz S, Collings N. Study of cycle-by-cycle air-to-fuel ratio determined from the exhaust gas composition and a novel fast response device based on a wide band lambda sensor. *SAE Technical Paper Series* 2008;01:2439.
- [45] Hayhurst AN, Parmar MS. Does solid carbon burn in oxygen to give the gaseous intermediate CO or produce CO₂ directly? Some experiments in a hot bed of sand fluidized by air. *Chemical Engineering Science* 1998;53(3):427–38.
- [46] Arthur JR. Reactions between carbon and oxygen. *Trans Faraday Soc* 1951;47:164–78.
- [47] Phillips R, Vastola FJ, Walker PL Jr. The thermal decomposition of surface oxides formed on Graphon. *Carbon* 1970;8(2):197–203.
- [48] Heuchamps C, Duval X. Effet des catalyseurs sur les caracteristiques cinetiques de la combustion du graphite. *Carbon* 1966;4(2):243–53.
- [49] Hayhurst AN, Tucker RF. The combustion of carbon monoxide in a two-zone fluidized bed. *Combustion and Flame* 1990;79(2):175–89.
- [50] Hayhurst AN. Does carbon monoxide burn inside a fluidized bed? A new model for the combustion of coal char particles in fluidized beds. *Combustion and Flame* 1991;85(1–2):155–68.
- [51] Gilliland ER. Fluidised particles. Davidson JF, Harrison D. Cambridge University Press, New York. 1963. *AIChE J* 1964;10(5):783–5.
- [52] Agarwal PK. The residence phase of active particles in fluidized beds of smaller inert particles. *Chemical Engineering Science* 1987;42(10):2481–3.
- [53] Ergun SJ. Kinetics of the reaction of carbon dioxide with carbon. *Phys Chem* 1956;60:480-5.
- [54] Laurendeau NM. Heterogeneous kinetics of coal char gasification and combustion. *Progress in Energy and Combustion Science* 1978;4:221-70.
- [55] Turnbull E, Kossakowski ER, Davidson JF, Hopes RB, Blackshaw HW, Goodyer PTY. Effect of pressure on combustion of char in fluidised beds. *Chem Eng Res Des* 1984;62:223-34.
- [56] Roberts GW, Satterfield CN. Effectiveness Factor for Porous Catalysts. Langmuir-Hinshelwood Kinetic Expressions. *Ind Eng Chem Fund* 1966;4(3):288–93.
- [57] Young JB, Todd B. Modelling of multi-component gas flows in capillaries and porous solids. *International Journal of Heat and Mass Transfer* 2005;48:5338–53.
- [58] Annamalai K, Ryan W. Interactive processes in gasification and combustion—II. Isolated carbon, coal and porous char particles. *Progress in Energy and Combustion Science* 1993;19(5):383–446.

- [59] Fuller EN, Schettler PD, Giddings JC. New method for prediction of binary gas-phase diffusion coefficients. *Ind Eng Chem* 1966;58:18–27.
- [60] Dennis JS, Lambert RJ, Milne, AJ, Scott SA, Hayhurst AN. The kinetics of combustion of chars derived from sewage sludge. *Fuel* 2005;84:117-26.
- [61] Marek E and Świątkowski B. Experimental studies of single particle combustion in air and different oxy-fuel atmospheres. *Applied Thermal Engineering* 2014;66(1–2):35-42.
- [62] Hecht ES, Shaddix CR, Molina A, Haynes BS. Effect of CO₂ gasification reaction on oxy-combustion of pulverized coal char. *Proceedings of the Combustion Institute* 2011;33(2):1699-1706.
- [63] Singer S, Chen L, Ghoniem AF. The influence of gasification reactions on char consumption under oxy-combustion conditions: Effects of particle trajectory and conversion. *Proceedings of the Combustion Institute* 2013;34(2):3471-3478.
- [64] Parmar MS, Hayhurst AN. The heat transfer coefficient for a freely moving sphere in a bubbling fluidised bed. *Chem Eng Sci* 2002;57:3485-94.
- [65] Paterson WR, Hayhurst AN. Mass or heat transfer from a sphere to a flowing fluid. *Chem Eng Sci* 2000;55:1925–7.
- [66] Hayhurst AN. The mass transfer coefficient for oxygen reacting with a carbon particle in a fluidized or packed bed. *Combustion and Flame* 2000;121(4):679–88.
- [67] Frossling, N. *Gerlands Beitr Geophys* 1938;52:170-5.
- [68] Hayhurst AN, Parmar MS. Measurement of the mass transfer coefficient and Sherwood number for carbon spheres burning in a bubbling fluidized bed. *Combust Flame* 2002;130:361–75.
- [69] Glicksman L, Lord W, Valenzuela J, Bar-Cohen A, Hughes R. *Am Inst Chem Eng Symp Ser* 1981;77:139.
- [70] Davidson JF, Harrison D. *Fluidized Particles*. Cambridge University Press, Cambridge UK. 1963.:21.
- [71] Darton RC, LaNauze RD, Davidson JF, Harrison D. Bubble growth due to coalescence in fluidised beds. *Trans I Chem E* 1977;55:274–80.

Appendix A: Determination of the thickness of the boundary layer, δ

Determining an appropriate value of the boundary layer thickness, δ , can be problematic; nevertheless it is a key parameter in Stefan-Maxwell problems. Paterson and Hayhurst [65] gave the following correlation to determine δ in terms of the Sherwood number, Sh

$$Sh = Sh_0 \left(1 + \frac{d_p}{2\delta} \right) \quad (\text{A.1})$$

where Sh_0 is the Sherwood number for the stagnant case, given for a fluidised bed by $Sh_0 = 2\varepsilon_{mf}$, with ε_{mf} being the voidage at incipient fluidisation. Eq. (A.1) was originally derived from first principles for equimolar counter-diffusion but it has been shown [66] to apply equally to non-equimolar problems. Many correlations are available in the literature for the determination of Sh based on bed parameters and most are modified forms of the Frössling equation [67] for mass transfer in a fluid medium, *i.e.* no particulate phase: $Sh = 2.0 + 0.69Re^{1/2}Sc^{1/3}$. Hayhurst and Parmar [68] have shown that, although the theoretical basis of these modified correlations is sound, they do not adequately match experimentally-measured values of Sh . Based on extensive experimental measurements of Sh for different temperatures, size fractions of sand, superficial velocities, and initial diameters of a graphite sphere, they found that Sh was best correlated by

$$Sh_{EMCD} = 2\varepsilon_{mf} + 0.61 \left(\frac{U_p d_p}{\nu} \right)^{0.48} \left(\frac{\nu}{D} \right)^{1/3} \quad (\text{A.2})$$

with $\varepsilon_{mf} = 0.4$ for particles of sand and U_p being the gas velocity in the particulate phase, given by [69]:

$$U_p = U_{mf}(1 - \varepsilon_b) \left\{ 1 - \frac{\pi}{2} \ln \left(1 - \frac{6\varepsilon_b}{\pi} \right) \right\}. \quad (\text{A.3})$$

Here, ε_b is the voidage due to bubbles in the fluidised bed and ν the kinematic viscosity of the gas. The bubble voidage was determined from the two-phase theory of fluidisation as:

$$\varepsilon_b = \frac{U - U_{mf}}{U_b} = \frac{H - H_{mf}}{H} \quad (\text{A.4})$$

where H and H_{mf} are the heights of the fluidised bed when fluidised, respectively, by superficial gas rates of U and U_{mf} , and the bubble rise velocity, $U_b = U - U_{mf} + 0.711(gd_{b,m})^{0.5}$ [70], where $d_{b,m}$ is the mean bubble diameter. An estimate of $d_{b,m}$ as a function of the height above the distributor plate, h , is obtainable from the correlation of Darton *et al.* [71]:

$$d_{b,m}(h) = 0.54(U - U_{mf})^{0.4} \left(h + 4\sqrt{A_0} \right)^{0.8} / g^{0.2}. \quad (\text{A.5})$$

Here, A_0 is the distributor area per orifice and can be approximated as zero for a porous plate distributor. In the model the mean bubble diameter was taken to be half the diameter of a bubble at the top of the sand ($h = H$).

Strictly speaking, the above correlation for Sh_{EMCD} , viz. Eq. (A.2), only really holds for the case of equimolar counter-diffusion of O_2 towards a reacting carbon particle and of CO_2 away from the particle, *i.e.* Reaction (2). However, if CO is the only product from oxidizing carbon, there is no longer equimolar counter-diffusion of the reactant O_2 and the product CO. If both CO and CO_2 are produced at or very close to the carbon particle, *i.e.* Reactions (1) and, or, (3), the error in assuming $Sh = Sh_{EMCD}$ is less than 10% [66]. Additionally, the CO produced during the combustion of carbon will, at least in principle, burn to CO_2 in a boundary layer around the particle. In that case the net effect is of CO_2 being a primary product of oxidation. However, it has been shown that the presence of sand around a burning carbon particle in a fluidised bed somewhat inhibits the oxidation of CO to CO_2 [45],[66]. For this work, a rigorous derivation was made to relate Sh and Sh_{EMCD} . It follows the line of the analysis of Hayhurst [66] but considers both CO and CO_2 as the products of combustion.

Firstly, if at the surface of a burning particle $\gamma = J_{CO}/J_{CO_2}$, then from Eq. (22) the molar fluxes of CO and CO_2 can be related, respectively, as $J_{CO_2} = -J_{O_2}/(\gamma/2 + 1)$ and $J_{CO} = -\gamma J_{O_2}/(\gamma/2 + 1)$. Now, treating the nitrogen in the air as the balancing component in the Stefan-Maxwell equations gives

$$C_T \frac{dy_{O_2}}{dr} = \frac{y_{O_2} J_{CO} - y_{CO} J_{O_2}}{D_{O_2,CO}^{Eff}} + \frac{y_{O_2} J_{CO_2} - y_{CO_2} J_{O_2}}{D_{O_2,CO_2}^{Eff}} - \frac{y_{N_2} J_{O_2}}{D_{O_2,N_2}^{Eff}}. \quad (A.6)$$

Here $D_{i,j}^{Eff} = D_{i,j} \varepsilon / \tau^2$ and it was assumed that the diffusivities $D_{i,j}$ are equal to some mean value of diffusivity. This assumption of equal diffusivities introduces only a slight error, swamped to a large extent by the uncertainty in determining the value of Sh from the available correlations. In this study and strictly for the determination Sh , the mean diffusivity for the experiments under air combustion was taken as $D = D_{O_2,N_2}$ while for oxy-fuel combustion $D = D_{O_2,CO_2}$.

Now, substituting the above correlations of J_{CO_2} and J_{CO} in terms of J_{O_2} and γ in Eq. (A.6) gives

$$J_{O_2} = - \frac{D \frac{\varepsilon}{\tau^2} C_T}{\left(1 + \frac{\gamma}{\gamma+2} y_{O_2}\right)} \frac{dy_{O_2}}{dr}. \quad (A.7)$$

The rate of consumption of carbon per particle is $Q = -\phi \pi d_p^2 J_{O_2}$, where ϕ is the stoichiometric coefficient of Reaction (23), $\phi = (\gamma+1)/(\gamma/2+1)$. Substituting for J_{O_2} in Eq. (A.7) and integrating from $r = d_p \rightarrow \infty$ and $y_{O_2} = y_{O_2,s} \rightarrow y_{O_2,bulk}$ on each side of the equation, the rate of consumption of carbon per particle, Q , can be rewritten as

$$Q = 4\pi d_p D \frac{\varepsilon}{\tau^2} C_T \frac{(\gamma+1)}{\gamma} \ln \left(\frac{1 + \frac{\gamma}{\gamma+2} y_{O_2,bulk}}{1 + \frac{\gamma}{\gamma+2} y_{O_2,s}} \right) \quad (A.8)$$

where $y_{O_2,s}$ and $y_{O_2,bulk}$ are the mole fractions of O_2 at the surface of the particle and in the bulk phase, respectively. This combustion rate was scaled by a factor of $(Sh_{EMCD}/Sh_0$ with $Sh_0 = \frac{\varepsilon}{\tau^2}$) to take account of the additional mass transfer by convection [66]:

$$Q = 2\pi d_p D C_T Sh_{EMCD} \frac{(\gamma+1)}{\gamma} \ln \left(\frac{1 + \frac{\gamma}{\gamma+2} y_{O_2,bulk}}{1 + \frac{\gamma}{\gamma+2} y_{O_2,s}} \right). \quad (A.9)$$

The mass transfer coefficient, k_g , can be defined by $Q = \phi \pi d_p^2 k_g \Delta C$ where ΔC is the change in the concentration of oxygen from the bulk flow to the surface of the char, *i.e.* $\Delta C = C_T (y_{O_2,bulk} - y_{O_2,s})$. Hence, in this case

$$k_g = \left(\frac{Sh_{EMCD} D}{d_p} \right) \left(\frac{\gamma+2}{\gamma} \right) \frac{1}{y_{O_2,bulk} - y_{O_2,s}} \ln \left(\frac{1 + \frac{\gamma}{\gamma+2} y_{O_2,bulk}}{1 + \frac{\gamma}{\gamma+2} y_{O_2,s}} \right) \quad (A.10)$$

and, as $Sh = k_g d_p / D$, the Sherwood number for the combustion of a char particle to a mixture of CO_2 and CO can be related to Sh_{EMCD} by

$$Sh = \left(\frac{\gamma+2}{\gamma} \right) \frac{1}{y_{O_2,bulk} - y_{O_2,s}} \ln \left(\frac{1 + \frac{\gamma}{\gamma+2} y_{O_2,bulk}}{1 + \frac{\gamma}{\gamma+2} y_{O_2,s}} \right) Sh_{EMCD}. \quad (A.11)$$

Eq. (A.1) can now be combined with Eqs. (A.2) to (A.5) and (A.11) to give a reasonable estimate of the boundary layer thickness, δ .

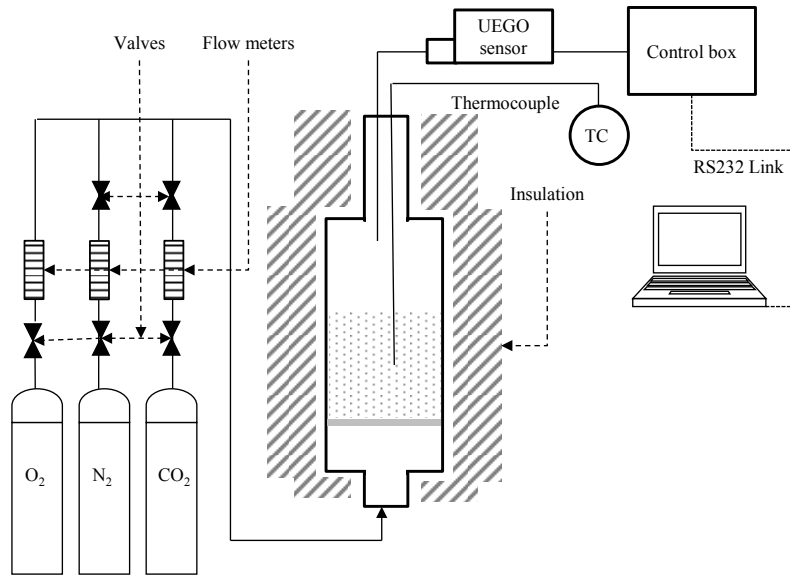


Figure 1.

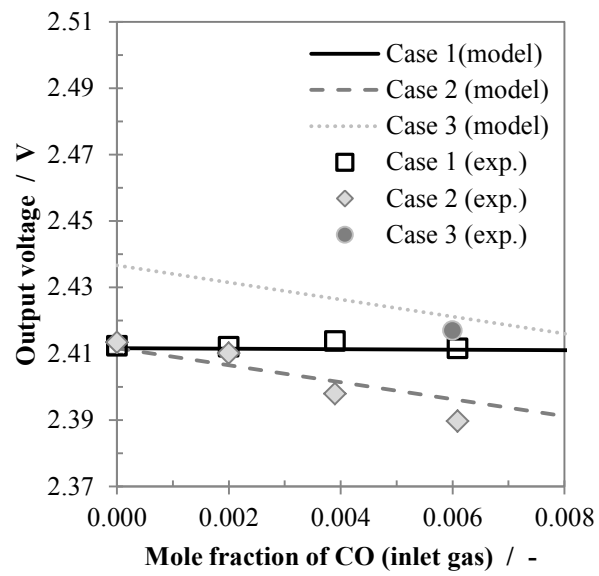


Figure 2.

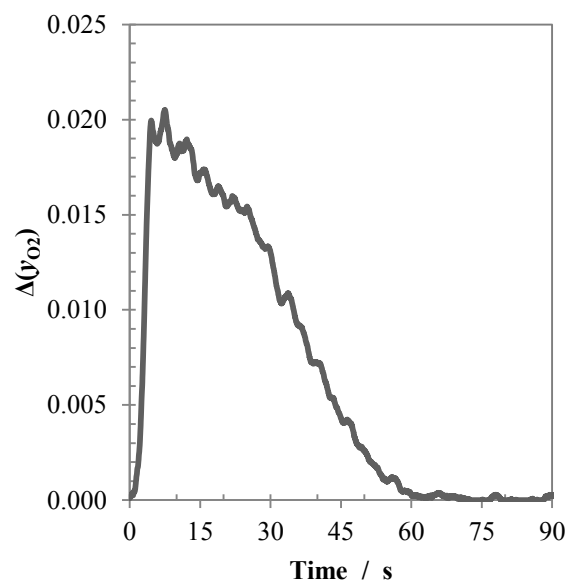


Figure 3.

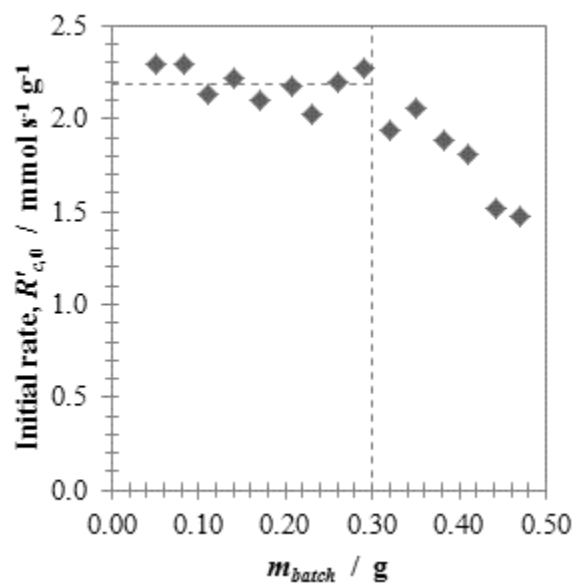


Figure 4.

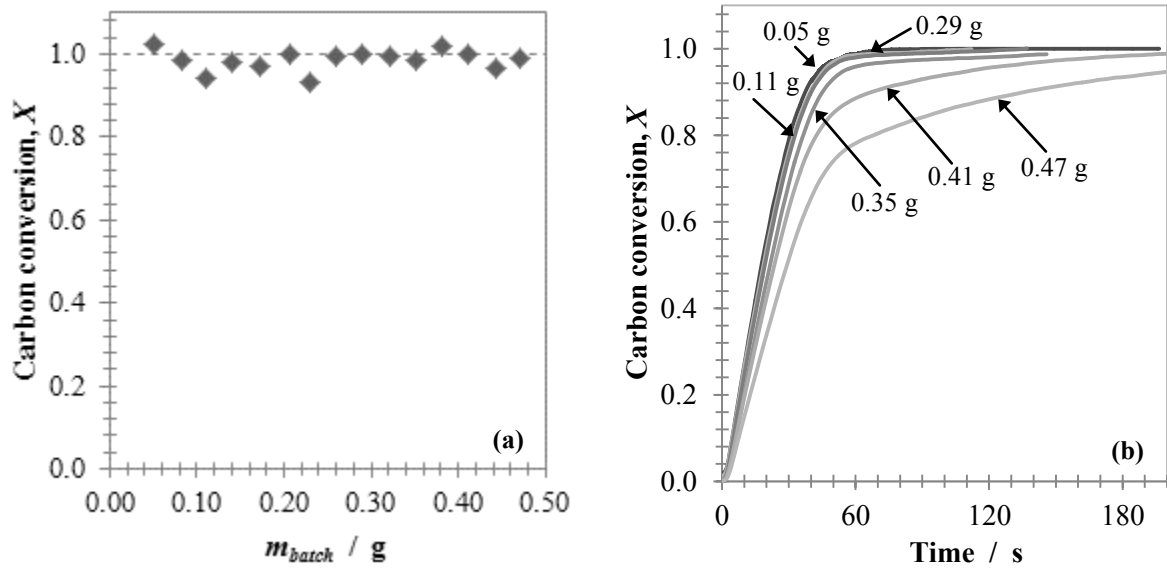


Figure 5.

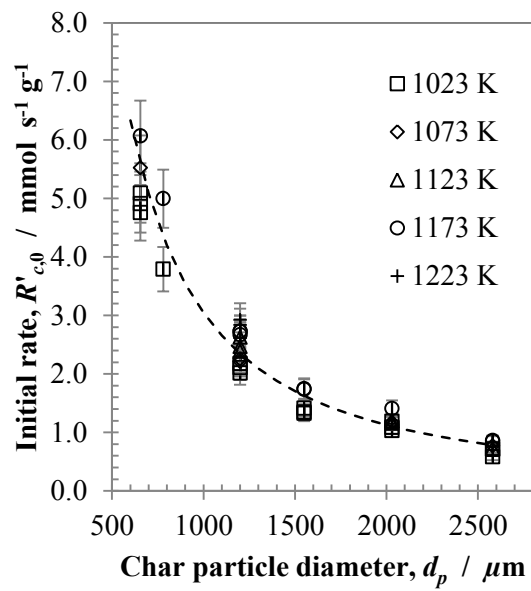


Figure 6.

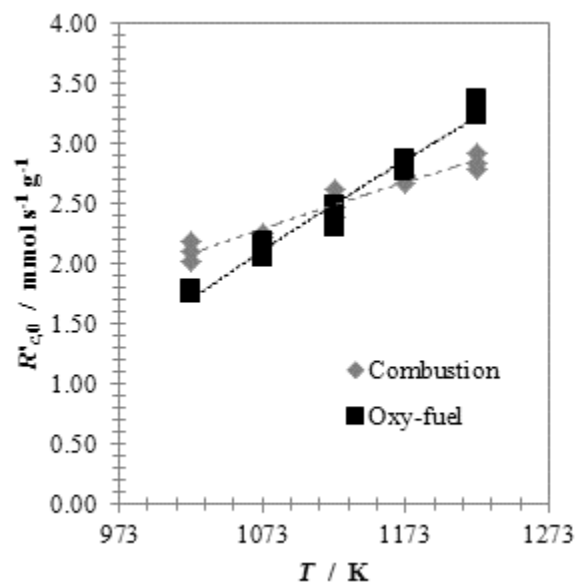


Figure 7.

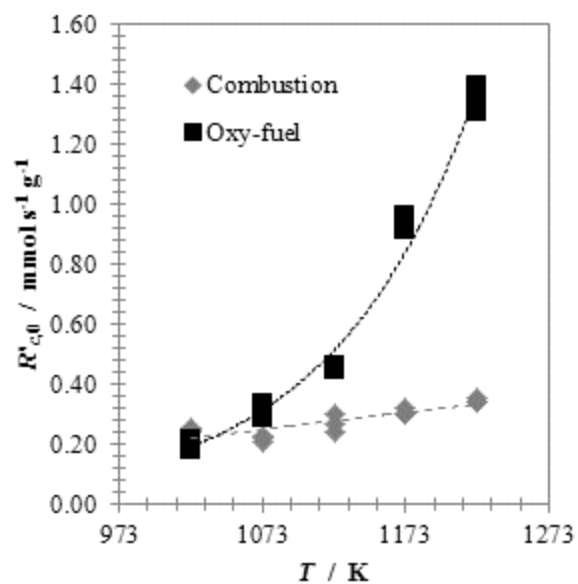


Figure 8.

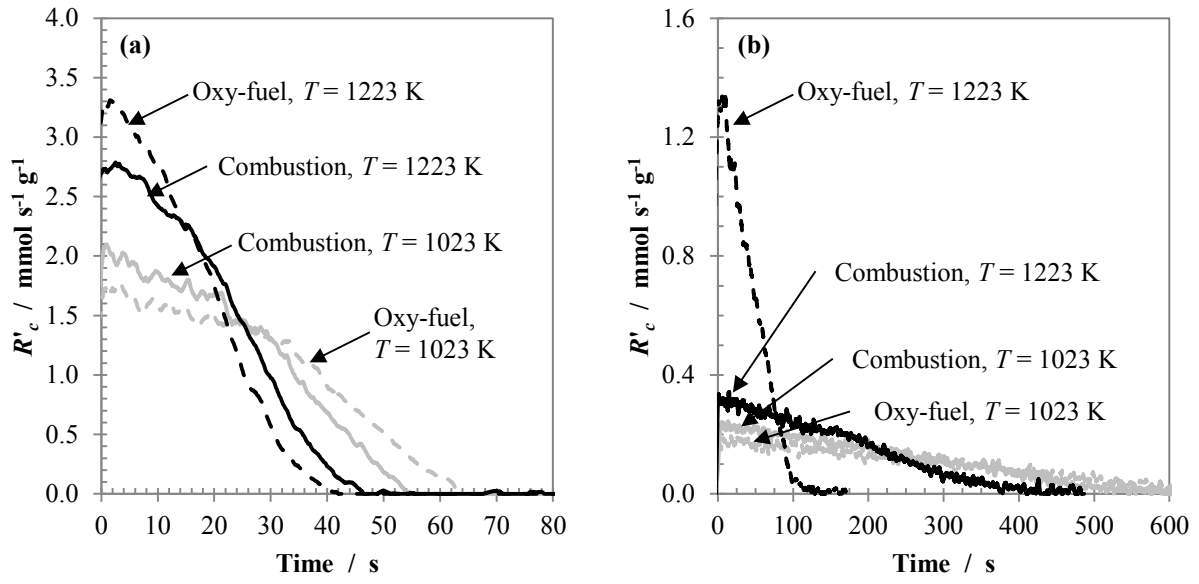


Figure 9.

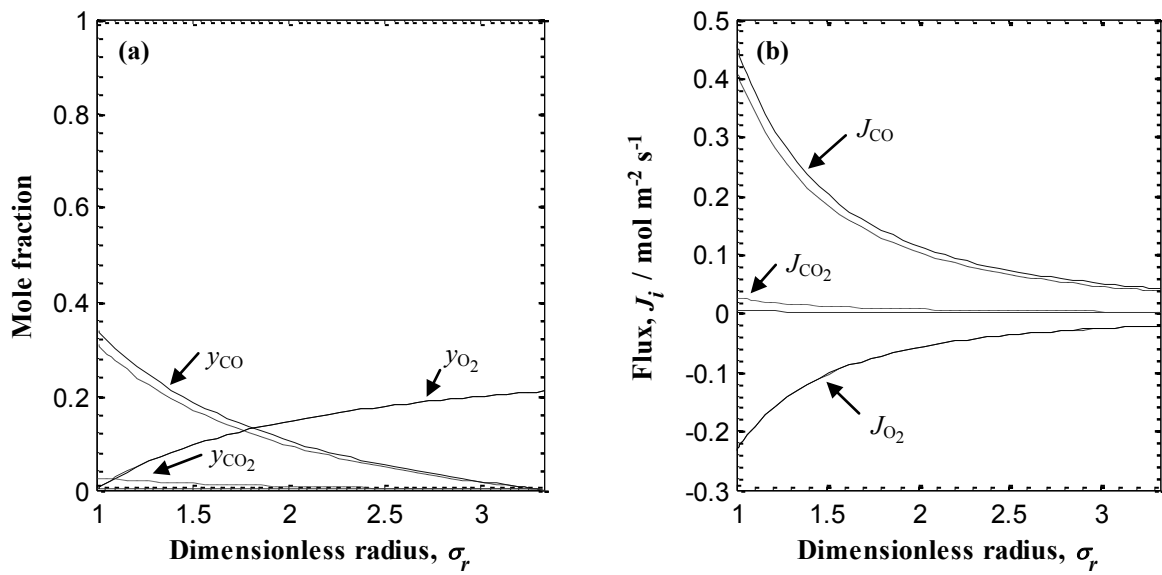


Figure 10.

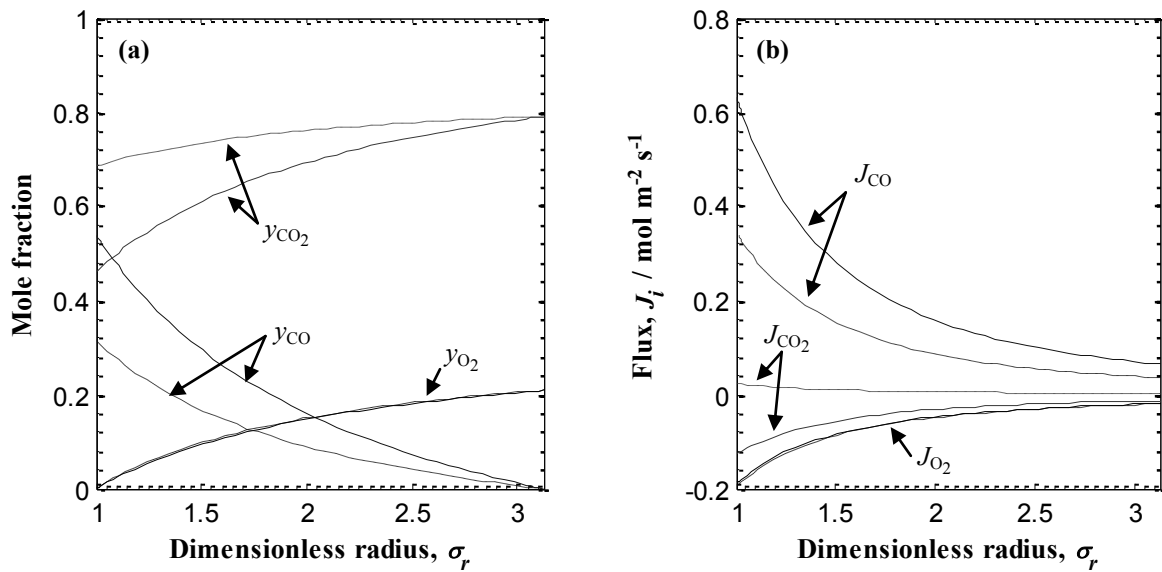


Figure 11.

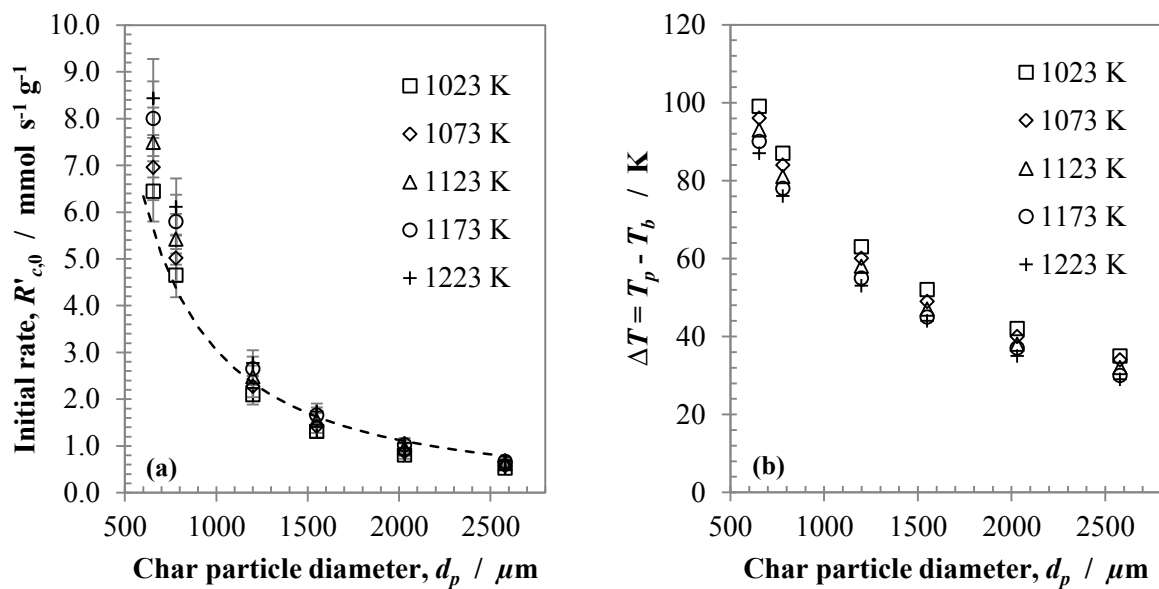


Figure 12.

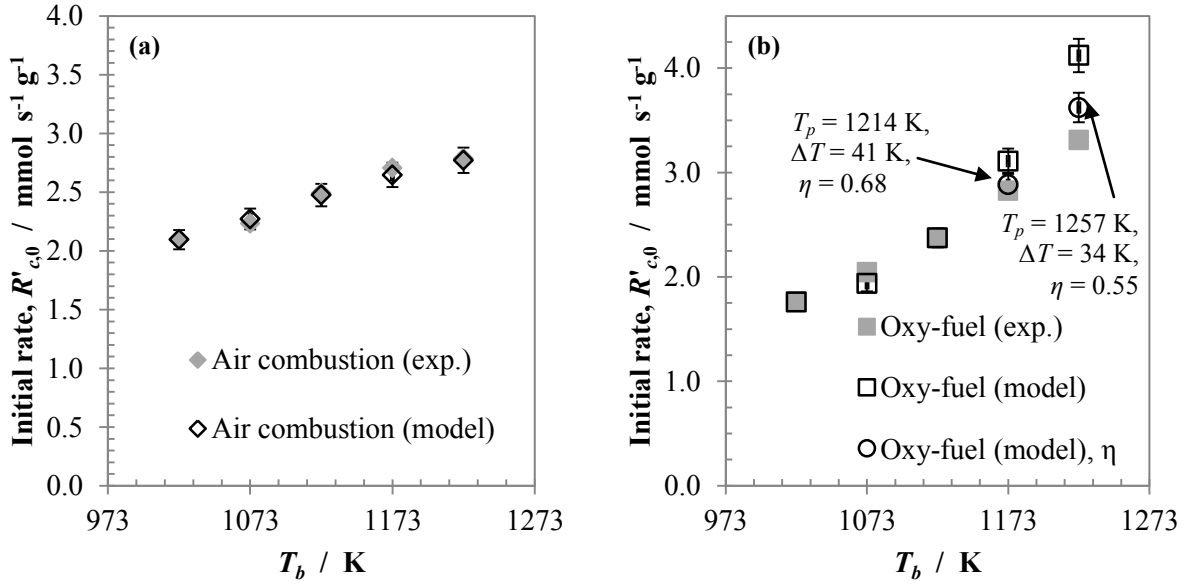


Figure 13.

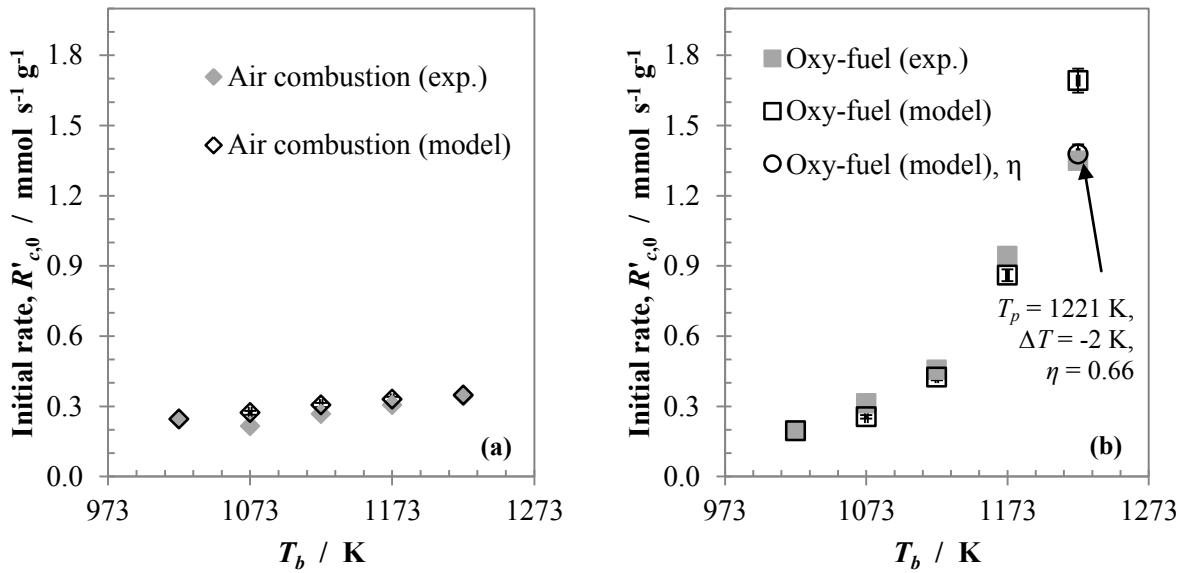


Figure 14.

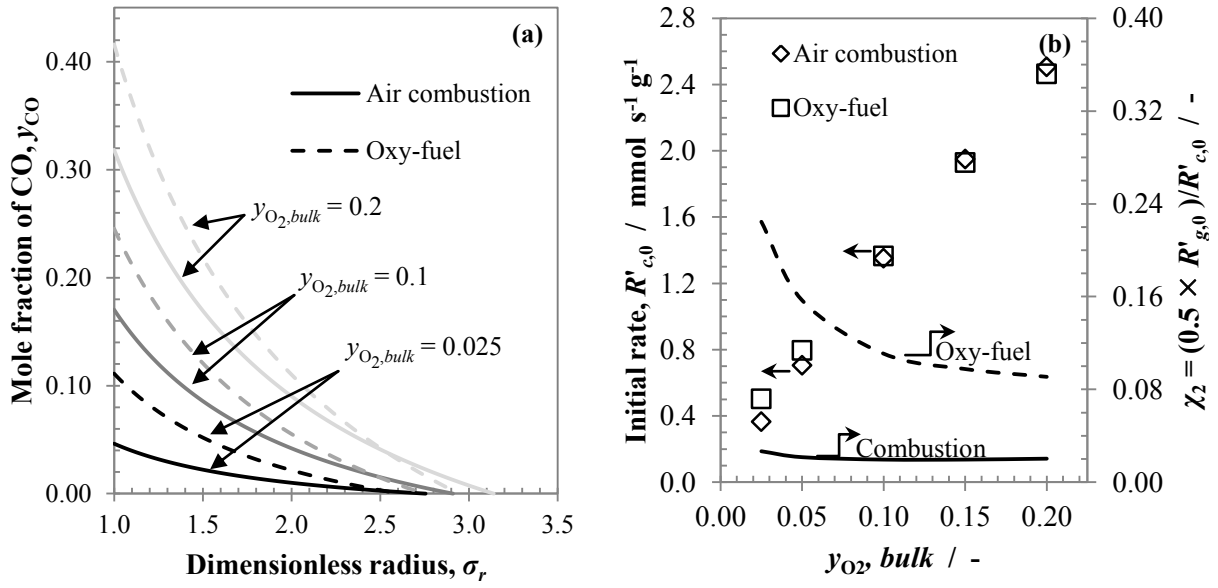


Figure 15.

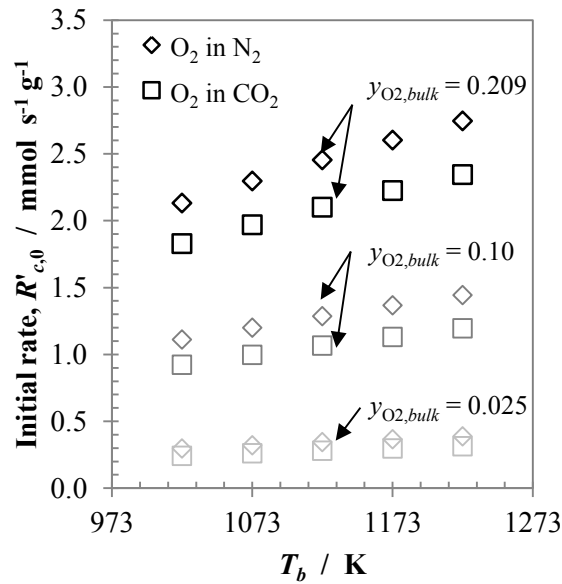


Figure 16.

Table 1.

Ash content and elemental analysis of Hambach lignite char.

Ash content	Elemental analysis				
	Sulphur	Carbon	Hydrogen	Nitrogen	Oxygen
8.76 wt.%	0.60 wt.%	85.69 wt.%	0.82 wt.%	0.84 wt.%	3.29 wt.%

Table 2.

Estimated intrinsic kinetic parameters in Eq. (8) and activation energy, E_{k_1/k_1} , in Eq. (9) in the study of gasification of Hambach lignite char by Saucedo *et al.* [35].

Parameter	Units	Value
T	K	1048 - 1248
d_p	μm	+600, -1000
$2ck_2$	$\text{mmol s}^{-1} \text{g}^{-1}$	$1.26 \times 10^{14} \exp[-34880/T]$
$2ck_1$	$\text{mmol s}^{-1} \text{g}^{-1} \text{bar}^{-1}$	$2.56 \times 10^9 \exp[-24050/T]$
k_2/k_1	bar	$4.92 \times 10^4 \exp[-10830/T]$
E_{k_1/k_1}	kJ mol^{-1}	-91.0